# Wheatstone Project

## Underwater Noise Monitoring and Review Program Results

| | | | | | |
|---|---|---|---|---|---|
| | | | | | |
| | | | | | |
| | | | | | |
| A | 24-May-2016 | Issued For Information | AG | CKVA | JSMQ |
| **REV** | **DATE** | **DESCRIPTION** | **ORIG** | **CHK** | **APPR** |

| | | | |
|---|---|---|---|
| **IP Security** | ☐ Company Confidential | **Total number of Pages (including Cover sheet):** | 44 |

| | | | |
|---|---|---|---|
| **For Contractor Documents** | **Contract No** | **Contractor Document No** | **Contractor Rev.** |
| | | CMST 1048 | 1 |

| **COMPANY DOCUMENT CONTROL No.** | **Project** | **Area** | **Discipline** | **Type** | **Originator** | **Package** | **Sequence-Sht** | **Revision** |
|---|---|---|---|---|---|---|---|---|
| | WS0 | 0000 | HES | RPT | CUR | 000 | 00004-000 | A |


**Centre for Marine Science and Technology**
**Curtin University**

# MODELLING AND MEASUREMENTS OF UNDERWATER NOISE FROM MARINE PILE DRIVING (Final Report)

Prepared for Chevron

Prepared by: Alexander Gavrilov, Daniel Wilkes and Marta Galindo Romero

Reviewed by:

PROJECT: CMST 1048

REPORT: 2016 – 1

January 2016

## Abstract

This report finalises the research project aimed to (1) develop a numerical model of underwater noise emission from marine pile driving, (2) validate this model by experimental measurements, (3) provide estimates for assessing potential impacts of piling noise on the local marine fauna of major concern (humpback whales, dolphins and turtles), and (4) compile a library of underwater sounds from marine pile driving for different distances and piling parameters, which can be used in the future for various environmental assessments. The numerical model of sound emission developed in the previous stage of the project is enhanced with a much more realistic physical model of hammer impacts. A comparison of numerical predictions for the major noise characteristics, such as the peak pressure and sound exposure levels, with the measurement data collected at the Wheatstone piling site demonstrates a satisfactory agreement. A library of underwater sounds from the Wheatstone piling operations has been compiled from data of a long-term underwater noise monitoring program and is described in the report. A new statistical approach is suggested and verified to predict the peak pressure level and its variation with greater confidence. The furthest distances of possible impacts of underwater piling noise on humpback whales, dolphins and turtles are estimated.

# Contents

# 1. Introduction

The material presented in this report summarises results of the project aimed to (1) develop a numerical model of underwater noise emission from marine pile driving, (2) validate this model by experimental measurements, (3) provide estimates for an assessment of potential impacts of piling noise on the local marine fauna of major concern (humpback whales, dolphins and turtles), and (4) compile a library of underwater sounds from marine piling for different distances and piling parameters, which can be used in the future for various environmental assessments.

The theoretical foundation and numerical approach implemented in the model of sound emission developed by the Centre for Marine Science and Technology (CMST) at Curtin University were described in detail in the previous reports on the project and in the recent publication by Wilkes *et al.*, 2016. This model has been benchmarked at the COMPILE workshop against state-of-the-art models from several international research teams (Lippert *et al*., 2016 and Wilkes *et al.*, 2016). The new achievement in the model development described in this report is a much more physically realistic model of hammer impact, compared to the COMPILE model, which has been verified by Pile Driver Analyser (PDA) data collected from the Wheatstone piling operation (Section 2.1).

Numerical predictions of the sound signal waveform, its peak pressure and sound exposure levels are compared with measurement data at short and long distances in Sections 2.2 and 2.3. The measurement data used for this comparison were collected during the near-field measurement program in the area of the Wheatstone jetty construction. Seafloor vibrations due to pile driving were also measured during this program and interpreted using a theoretical approach (Section 2.2)

Long-term measurements from November 2014 to August 2015 to monitor noise from the Wheatstone piling operations are described in Section 3.1. This monitoring program has resulted in a library of underwater sounds from marine pile driving, which is described in Section 3.2.

Analysis of the piling noise measurements made during the long-term monitoring program has resulted in some new findings related to the prediction of the peak pressure level in impulsive signals from pile driving and its fluctuations due to environmental variations. A statistical approach based on extreme value theory was used to model such fluctuations and predict the probability of the peak pressure level to be below or exceed a chosen threshold. This is presented in Section 3.3.

A noticeable difference between the underwater sound levels from vertical and slanting piles, driven to construct the Wheatstone jetty, was observed in the long-term noise monitoring data, which is another important finding relevant to environmental assessments, as discussed in Section 3.4.

The furthest distances of various possible impacts of piling noise on the marine animals of concern are estimated in Section 4. These impacts include possible injuries to animals hearing, Temporal hearing Threshold Shift (TTS) onset and behavioural disturbance. The estimates are compared to those made by SVT as part of the preliminary environmental assessment program (Chevron, 2011). Finally conclusions are made in Section 5 along with some recommendations for the future studies.

# 2. Experimental verification of the underwater sound emission model by impact pile driving

## 2.1 Model of impact force and its experimental verification

A combined Finite Element Method (FEM) and Normal Mode (NM) model for numerical predictions of the sound field at short and long distances from an impact driven pile was described in detail in the previous reports on the project and, more recently, in Wilkes at al., 2016. However, in the previous modelling studies a simple, rather notional model of impact force produced by a hammer strike was employed based on the COMPILE benchmark test scenario (Lippert et al, 2016).

To verify the numerical model of underwater noise emission from marine pile driving using experimental measurements of underwater noise recorded from the piling operations within the Wheatstone project, a much more physically realistic model of impact force was suggested and verified. The model is based on an analytical solution made by Deeks and Randolph (1993) for a ram-cushion-anvil system with some minor alterations implemented to avoid complex roots in the solution and to correct some errors in formulation. Although the IHC hydrohammers used for pile driving at Wheatstone do not have a separate cushion, the ram-cushion-anvil model was chosen to allow for finite stiffness of the piston rod which is part of the ram striking the anvil (see Figure 2.1).

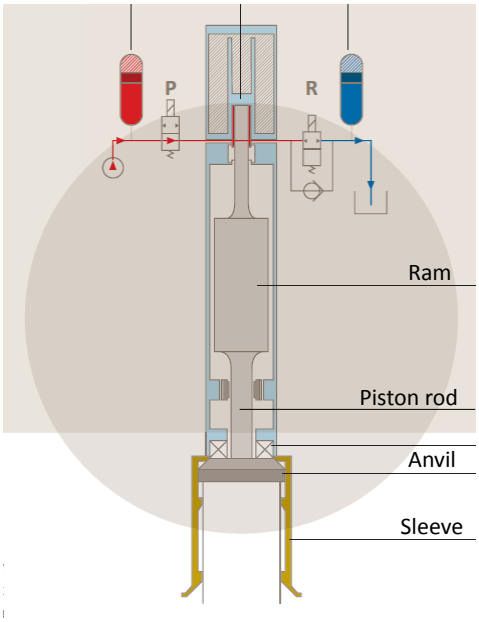


*Figure 2.1: Schematic of typical HTC hydrohammer design*

The hammer impact is modelled as a vertical time-dependent force $F_p(t)$ applied to the top of the pile. It is convenient to formulate the solution in terms of dimensionless force $F_d(t)$:

$$F_P(t) = Zv_0 F_d(t)\,, \qquad (2.1)$$

where $Z = EA/c_P$ is the pile mechanical impedance, $v_0$ is the ram velocity at impact, $E$ is the Young's modulus of the pile material, $A = 2\pi Rh$ is the cross-section area of the pile, $c_P$ is the axial compressional wave velocity in the pile, $R$ is the pile radius, and $h$ is the wall thickness. The other parameters are also represented in dimensionless units as follows: $t_d = tZ/M$ is dimensionless time, where $M_R$ is the ram mass; $k_d = kM_R/Z^2$ is dimensionless stiffness of the cushion, and $M = M_A/M_R$ is a ratio of the anvil and ram mass.

The velocity $c_P$ can be calculated from the pile parameters as:

$$c_P = \left( \frac{E}{\rho\left(1-\eta^2\right)} \right),$$

where $\rho$ is density of pile material and $\eta$ is its Poisson's ratio.

By introducing the following variables:

$\alpha = a_1 a_2 / 6 - a_0 / 2 - a_2^3 / 27$ and

$\beta^2 = a_1^3 / 27 - a_1^2 a_2^2 / 108 - a_0 a_1 a_2 / 6 + a_0^2 / 4 + a_0 a_2^3 / 27$,

where $a_0 = k_d / M$, $a_1 = k_d\left(1/M + 1\right)$ and $a_2 = 1/M$, the solution for the dimensionless force function $f_p(t_d)$ can be found in the following form:

$$F_d\left(t_d\right) = \frac{a_0}{\omega^2 + c^2} \exp\left(-b_1 t_d\right)\left[1 - \exp\left(-ct_d\right)\cos\left(\omega t_d - \varphi\right)/\cos\varphi\right], \qquad (2.2)$$

where

$$\omega = \frac{3^{1/2}}{2}\left[\left(\alpha+\beta\right)^{1/3} + \left(\beta-\alpha\right)^{1/3}\right],$$

$$c = b_2 - b_1,$$

$$\varphi = \tan^{-1}\left(c/\omega\right),$$

$b_1 = a_2/3 - \left(\alpha+\beta\right)^{1/3} + \left(\beta-\alpha\right)^{1/3}$, and

$b_2 = a_2/3 + \left(\alpha+\beta\right)^{1/3} - \left(\beta-\alpha\right)^{1/3}$.

Equation 2.2 is correct when the ram is in contact with the anvil. However, for certain combinations of the ram and anvil mass and stiffness *k*, the ram will separate from the anvil at a certain time $t_s$, after which the force function applied to the pile top will also change as follows:

$$F_d\left(t_d\right)\big|_{t>t_s} = F_d\left(t_d\right)\big|_{t=t_s} \exp\left(-\frac{t_d - t_{dsep}}{M_A}\right), \qquad (2.3)$$

where $t_{dsep} = t_s Z/M$.

The separation time $t_{dsep}$ is found when the force $F_R$ applied by the ram to the anvil becomes zero:

$$F_R\left(t_{dsep}\right) = M_A U\left(t_{dsep}\right)\frac{a_0}{\omega^2 + c^2} + F_P\left(t_{dsep}\right) = 0,$$

where

$$U\left(t_d\right) = \exp\left(-b_1 t_d\right)\left\{-b_1 y + \frac{\exp\left(-ct_d\right)}{\cos\varphi}\left[c\cos\left(\omega t_d - \varphi\right) + \omega\sin\left(\omega t_d - \varphi\right)\right]\right\}.$$

In the suggested physical model, almost all input parameters are usually known. The ram velocity at impact can be derived from the impact energy and ram mass. Pile parameters (material, radius and wall thickness) are also usually known. With respect to the hammer design shown in Figure 2.1, the only uncertain parameter is the stiffness of the piston rod.

To validate this numerical model of the impact force, it was used to calculate the stress and force along the pile as a function of time after impact using the Final Element Method (FEM) implemented in Program for Automatic Finite Element Calculations (PAFEC, http://www.vibroacoustics.co.uk/fe/fsfe.htm), and then the numerical result was compared with the force measurements made using strain gauges at 3.5 m below the pile top. A comparison of modelling results with the measurements is shown in Figure 2.2 for two different piles driven with impact energy of 270 kJ and 198 kJ.

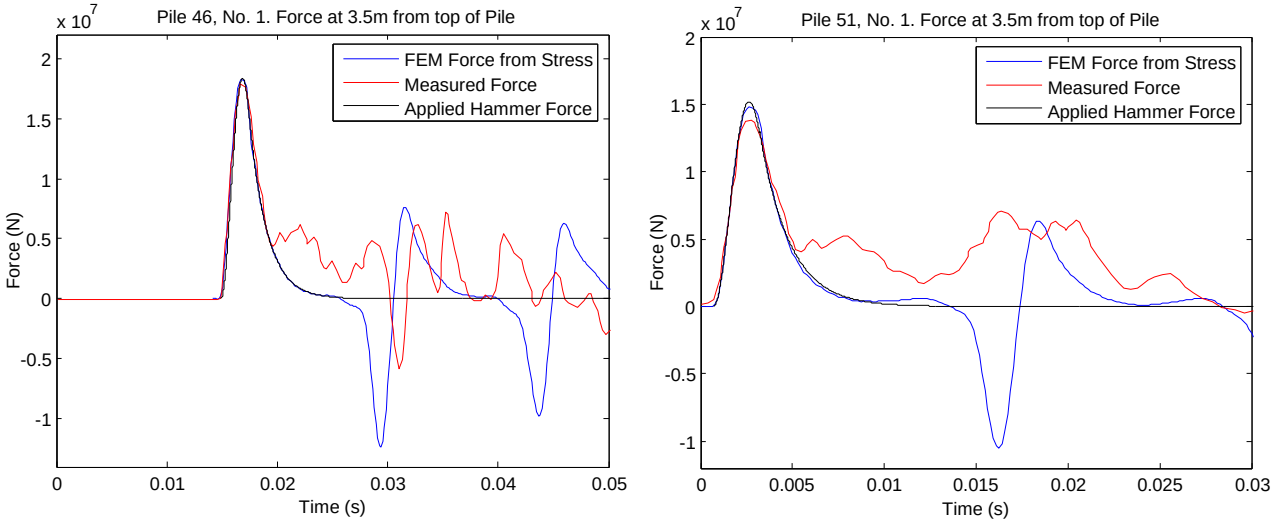


*Figure 2.2: Measured (red) and modelled (blue) force at 3.5 m below the pile head for impact energy of 270 kJ (left) and 198 kJ (right). The black line shows the model prediction for the force applied to the pile head in vacuo.*

The numerical modelling was performed for the hammer and pile parameters given in Table 2.1. The hammer parameters were taken from specs of an IHC Hydrohammer S-280 used for the Wheatstone jetty pile driving. The only unknown parameter varied to fit the measured force was the stiffness coefficient $k$. The best-fit value of $k = 8 \cdot 10^9$ N/m is reasonable. For example, this value corresponds to axial stiffness of a steel cylindrical rod of 0.5 m length and 15 cm diameter.

*Table 2.1: Hammer and pile parameters used for modelling*

| $R$ [mm] | $h$ [mm] | $\rho$ [kg/m3] | $E$ [Pa] | $\eta$ | $M_R$ [kg] | $M_A$ [kg] | $k$ [N/m] |
|---|---|---|---|---|---|---|---|
| 1016 | 22 | 7850 | $210 \cdot 10^9$ | 0.3 | 14000 | 4400 | $8 \cdot 10^9$ |

As can be seen in Figure 2.2, the model predicts accurately the amplitude and shape of the primary impact impulse. However, the tails of the measured and modelled force impulses are different. PAFEC-FE does not predict the reflection of the displacement and force impulse from the air-water interface, which is seen in the measurement data at about 5ms after the impulse start time. This is not related to the impact force model given in Eqs. 2.1-3, but is most likely a consequence of how PAFEC-FE treats the boundary conditions. The signal arriving after approximately 15 ms is due to the reflection from the pile toe. It also looks different in the measured and modelled waveforms. The major cause of this difference is most likely an oversimplified model of the seabed (see next section) compared to a complex layered structure of the sediments observed in borehole probes.

## 2.2 Near-field results

### *Underwater sound signals*

Underwater noise from the piles driven during the construction of the Wheatstone jetty was recorded at short distances as part of the near-field measurement program. The piling noise was recorded on two bottom-mounted sea noise recorders (noise loggers) combined with 3C seismometers and deployed from the 14th of April to the 13th of May 2015 at the locations shown on the bathymetry map in Figure 2.3. The mooring design is described in Gavrilov *et al.* (2014). Twelve piles were driven during the near-field measurement program; however, only two piles specified as PI-TR-46-01 and PI-TR-56-01 were used for comparison of measured and numerically predicted sound signals from pile driving. These piles were chosen because: (1) the recorded signals were not clipped in the sound recording system due to an excessively high sound pressure of piling signals at short distances, (2) the sound from these piles was also recorded on a noise logger deployed at about 2 km offshore as part of the long-term noise monitoring program, and (3) both piles were vertical. The other piles recorded during the near-field measurement program were either slanting (raker), for which a numerical model of sound emission is not developed yet, or were driven too close to the near-field loggers such that the recorded signals were clipped. The relevant pile and driving parameters are given in Table 2.2.

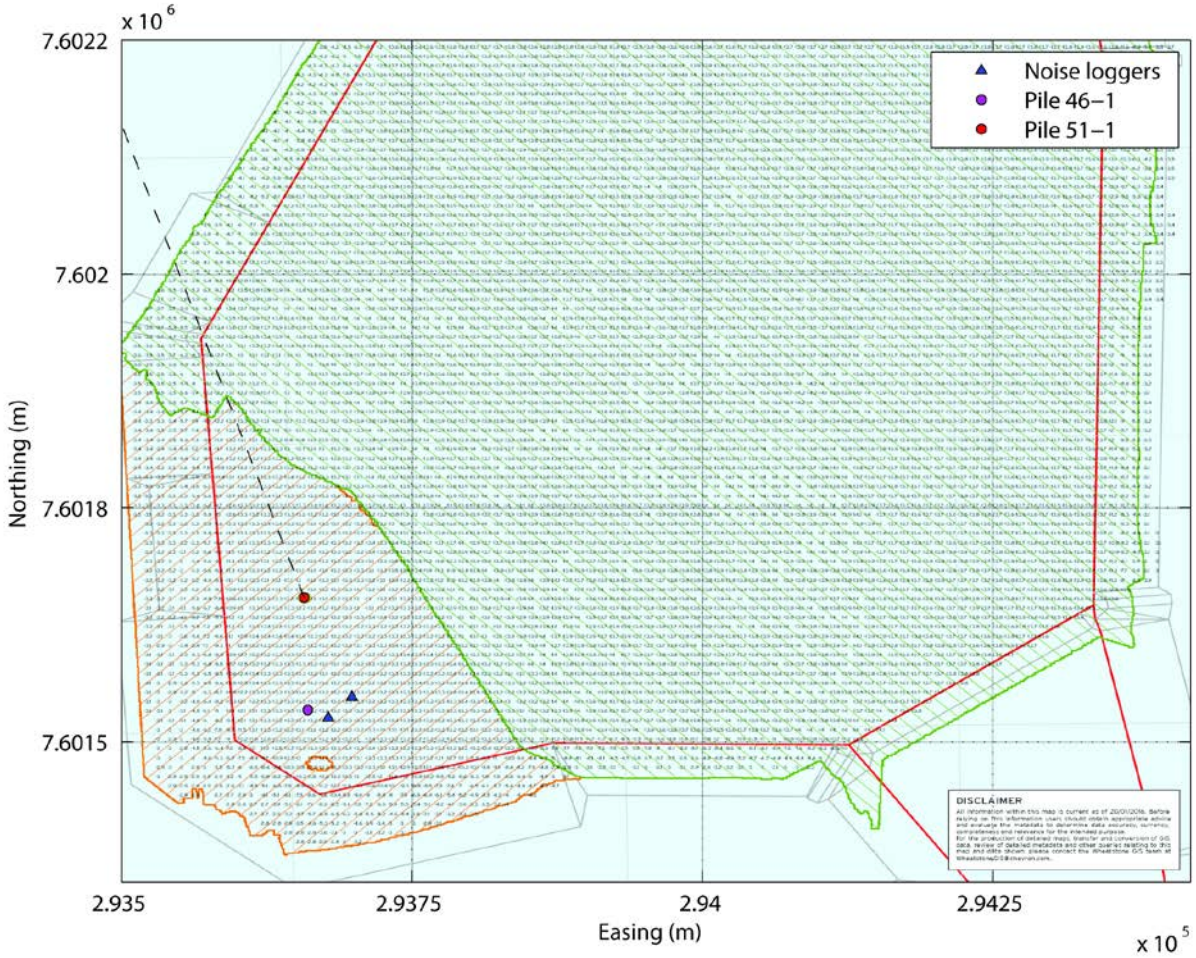


*Figure 2.3: Fine bathymetry map of the dredged area around the Wheatstone turning basin drawn from multi-beam sonar data. Red and magenta circles show the location of piles 51-01 and 46-01 respectively. Triangles show the location of the noise loggers. Dashed line indicates the direction to the far-field logger (#2 in Table 3.1) from pile 51-01.*

Underwater sound signals from the two piles were modelled using the FEM model described in detail in the previous report on the project (Gavrilov *et al*., 2014) and in Wilkes *et al*. (2016).

*Table 2.2: Relevant pile and driving parameters used for modelling*

| Pile ID | Diameter [mm] | Wall thickness [mm] | Length [m] | Ground penetration [m] | Sea depth [m] | Hammer energy [kJ] | Blow rate [b/min] |
|---|---|---|---|---|---|---|---|
| 46-01 | 1016 | 22 | 37.5 | 9.65 | 14.36 | 270 | 28 |
| 51-1 | 1016 | 22 | 40 | 8.5 | 15.35 | 198 | 42 |

The borehole probes taken from the area of pile driving before dredging of the turning basin (boreholes MT-308 to MT310 in Golder Associates, 2011) showed that the sediments in the top 15 to 20 m of ground were unconsolidated, unevenly layered and consisting of varying fractions of sand and clay overlaying a basement of cemented sediments, such as claystone and sandstone. The thickness of this soft sediment layer has reduced to 8-12 m after dredging. Because the final ground penetration of the jetty piles (see Table 2) was comparable to the thickness of unconsolidated sediments, it was assumed in the FEM model that the underground section of piles remained in the soft sediment layer, where the effect of shear in the sediment material could be ignored. To further simplify the numerical model, the effect of the underlying basement of hard material on sound emission was also ignored. Finally, the bottom was modelled as homogeneous sediment material, because the contrast between soft sediment layers was not very high in terms of their contents. The geoacoustic parameters of the sediment were assumed to be similar to those of medium grain-size sand: having a bulk density of 1850 kg/m$^3$, compressional wave velocity of 1800 m/s, and compressional wave attenuation of 0.47 dB/$\lambda$.

Figures 2.4 to 2.6 show a comparison of the numerically predicted and measured waveforms of underwater signals from two piles received at the bottom at three different distances from the pile.

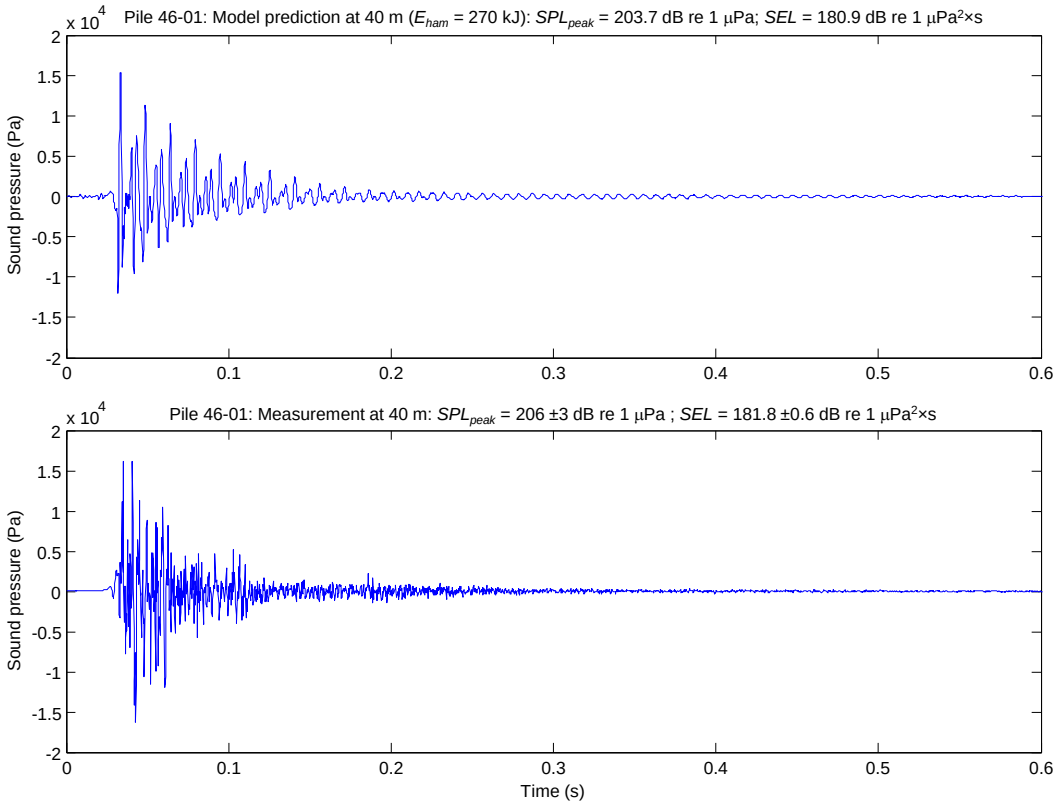


*Figure 2.4: Waveform of an underwater sound signal from a single blow modelled (top) and measured (bottom) at the bottom at a distance of 40 m from pile 46-01.*

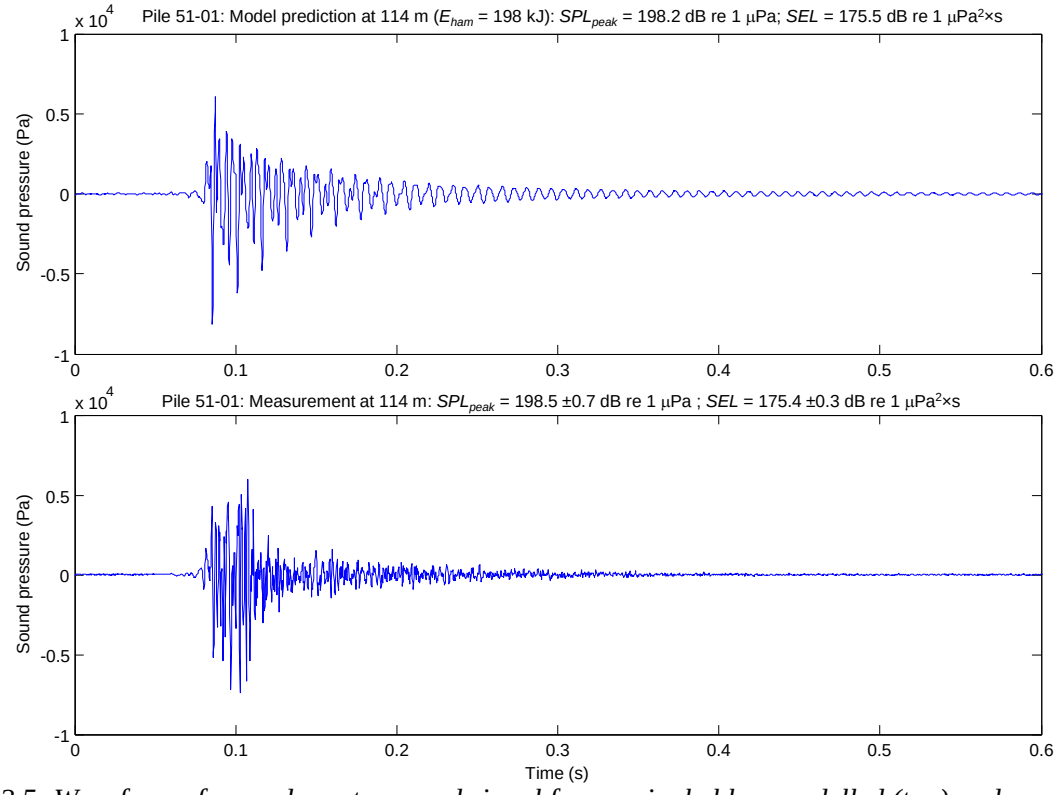


*Figure 2.5: Waveform of an underwater sound signal from a single blow modelled (top) and measured (bottom) at the bottom at a distance of 114 m from pile 51-01.*

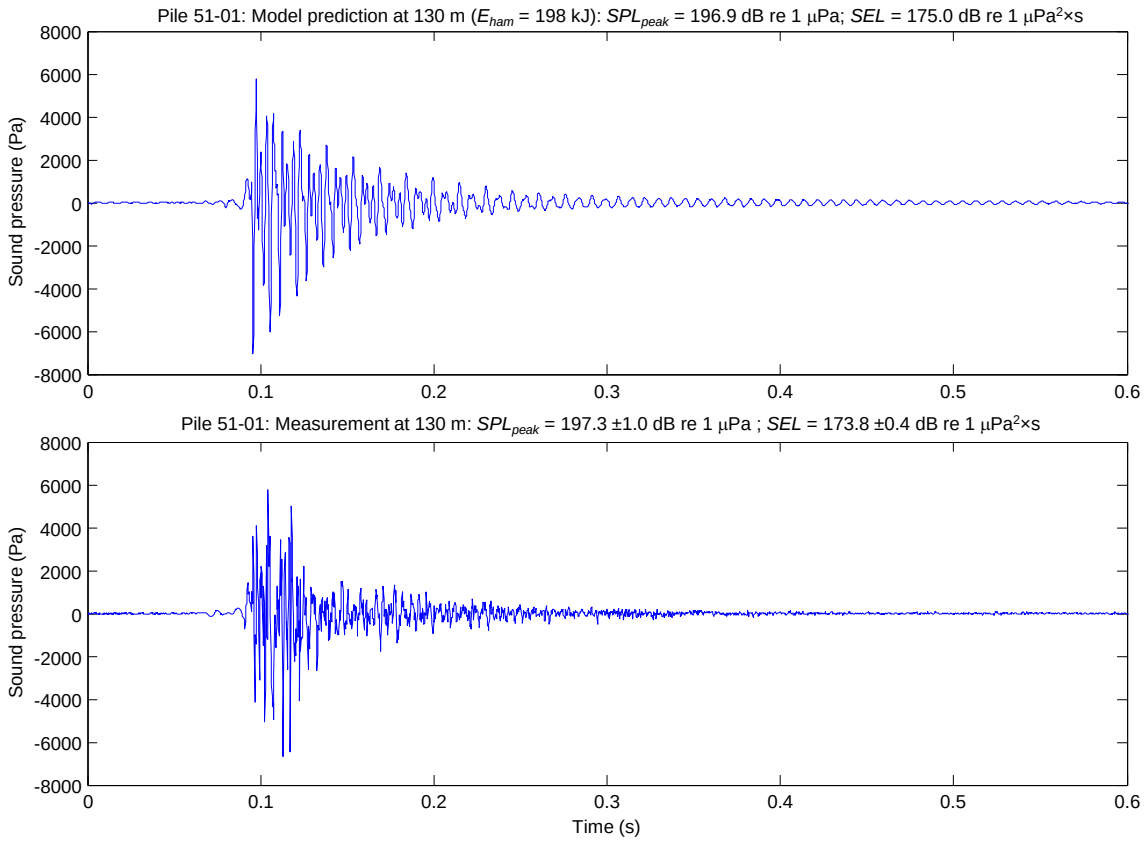


*Figure 2.6: Waveform of an underwater sound signal from a single blow modelled (top) and measured (bottom) at the bottom at a distance of 130 m from pile 51-01.*

Although the modelled and measured waveforms look somewhat different in details, the major characteristics, such as the maximum amplitude and decay, are similar. The similarity is also evident from the comparison of the Sound Exposure Level (*SEL*) and peak pressure level ($SPL_{peak}$). The measured levels varied between strikes, so the mean value and standard deviation were calculated for multiple strikes, which are shown in the plot headers. The numerically predicted values of $SPL_{peak}$ and *SEL* are within the standard deviation of the measured data, except for the last case (Figure 2.6) where the predicted *SEL* value is about 1 dB lower than the measurement.

The most noticeable difference between the modelled and measured waveforms is the presence of obvious low-frequency oscillations in the modelled signal decaying with time. The period of oscillations corresponds to the one-way travel time of the impact wave along the pile, so these oscillations can be referred to as pile ringing. The ringing effect is not pronounced in the measured signals most likely because of friction between the pile wall and ground, which is not adequately modelled in the FEM model where the effect of damping due to friction is simulated via an artificial increase of compressional and shear wave damping in the pile material below ground (see Wilkes *et al*., 2016 for details).

### *Seafloor vibrations*

Results of numerical modelling, presented in Gavrilov *et al*., 2014 and Wilkes & Gavrilov, 2016, show that a pile driven into sediments with elastic properties supporting shear waves produces an interface wave which results in vibrations of the seafloor. This has been previously observed in experimental measurements (Hazelwood & Macey, 2012 and Reimann & Grabe, 2014). To examine this effect, the two noise loggers deployed on the seabed in the near field were modified at the CMST to combine them with 3-component (3C) seismometers. The seismometers consist of three geophones with preamplifiers to measure ground velocities along two perpendicular horizontal (*x* and *y*) and one vertical (*z*) axes. As the orientation of the seismometers relative to the direction of wave propagation from different piles was different, the horizontal component of ground velocity of interface waves in the direction of wave propagation was calculated using phase difference between the *x* and *y* components. The waveform of the vertical and horizontal components of ground velocity recorded at a distance of 130 m from pile 51-01 is shown in Figure 2.7 along with the sound pressure signal recorded by the hydrophone.

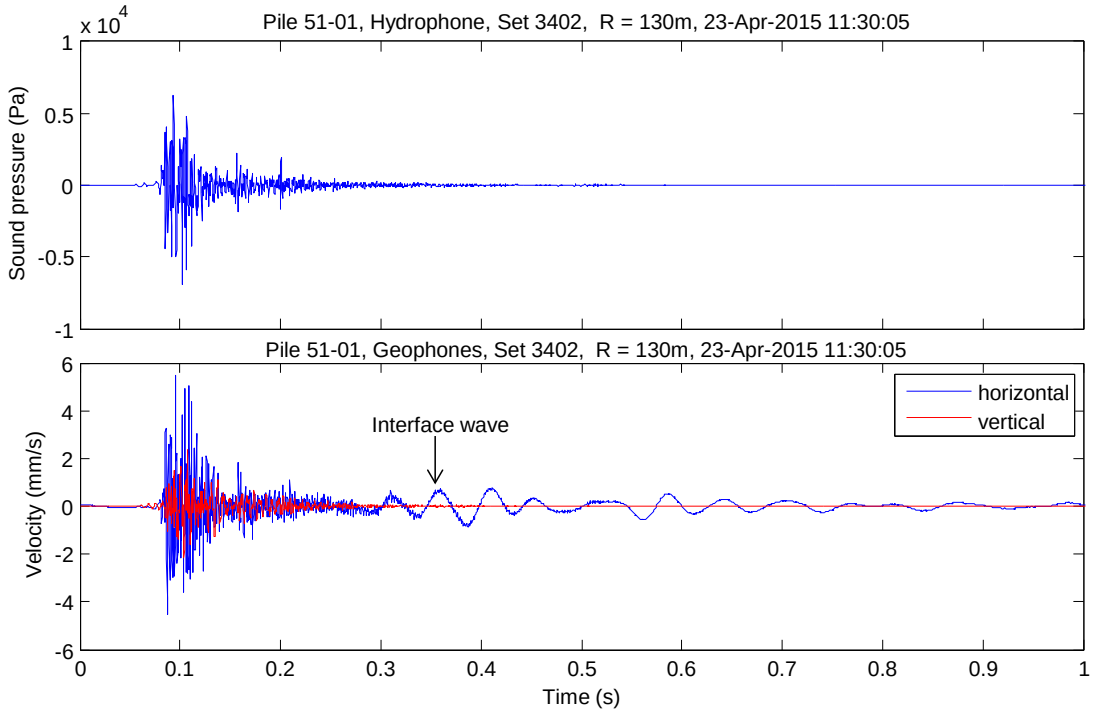


*Figure 2.8: Waveforms of sound pressure (top panel) and two components of ground velocity (bottom panel) from a single strike of pile 51-01 recorded by the noise logger with 3C seismometer at 130 m from the pile.*

The plot on the bottom panel of Figure 2.8 reveals a low frequency signal of horizontal displacement arriving about 200 ms later than the waterborne wave of much broader frequency band. The travel velocity of this wave is about 430 m/s. The most likely origin of the slowly propagating signal is an interface wave propagating along the water-sediment interface. The frequency band of this signal is very narrow and limited to approximately 20 Hz. At such low frequencies, the wavelength in water is significantly larger than the sea depth of about 15 m. This means that the interface wave should tend to have characteristics of a Rayleigh wave propagating along a pressure released surface of an elastic solid half-space rather than a Scholte wave propagating along a fluid-solid interface. This also means that the top 8-12 m layer of unconsolidated sediments also had shear stress. If the shear wave velocity in the top sediment was

about 450 m, then the Rayleigh wave velocity would be about 430 m/s at the compressional wave velocity in the sediment of 1800 m/s.

To verify this by numerical modelling, a point sound source was placed on the bottom at sea depth of 15 m and the force function shown in Figure 2.2 was taken as a source signal. Then the sound and particle velocity fields were calculated using a wavenumber integration method (Jensen *et al*., 2011). Figure 2.9 shows the waveform of sound pressure at the bottom and the horizontal (radial) and vertical components of ground velocity calculated at a distance of 130 m. The plot clearly shows the arrival of an interface wave at about the same time (~0.3s) as the low-frequency wave shown in Figure 2.8. The signal is noticeably shorter than that in the recorded waveform because the modelled source signal consists of only one impulse, while the signal emitted by a pile is formed by wall deformation waves traveling along the pile down and up several times.

It is much less certain why the vertical component of ground velocity is absent (or very small) in the measured data, while it is comparable to the horizontal component in the model. A similarly small vertical component of ground interface waves from marine pile driving has been observed in the other experimental measurements (e.g. Hazelwood & Macey, 2014). This is likely a result of a specific mechanism, through which a driven pile emits elastic waves in the ground, which should be investigated in future modelling studies.

Finally, it is important to notice that the amplitude of seabed vibrations due to interface waves observed in the Wheatstone data was significantly lower than that produced by the waterborne acoustic waves at the bottom.

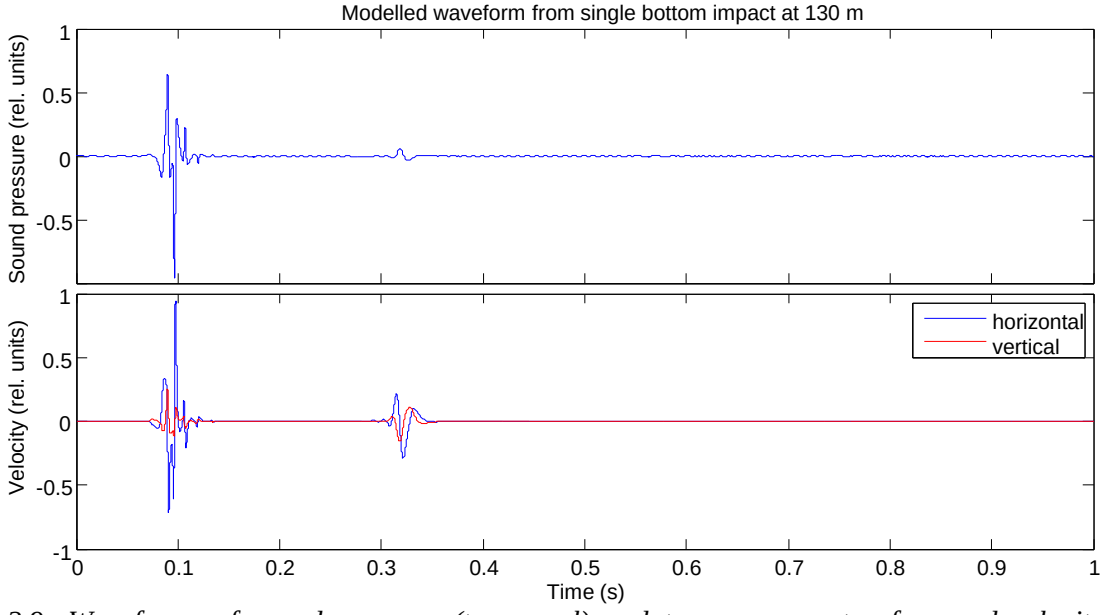


*Figure 2.9: Waveforms of sound pressure (top panel) and two components of ground velocity (bottom panel) modelled at the bottom at a distance of 130 m from a point source also placed on the bottom. The source signal used in the model is shown by the black line in Fig.2.2, left panel.*

## 2.3 Far-field results

Before carrying out numerical predictions of underwater sound signals from pile driving in the far field to make a comparison with the measurements, the near-to-far field coupling method via normal mode (NM) expansion, described in Gourlay & Gavrilov (2013) and Wilkes *et al.* (2016), was numerically tested. The sound field from a driven pile was modelled with FEM in the frequency domain in the near field up to a distance of 130 m from the pile. Parameters of pile 51-01 were used for modelling. Then the vertical sound field profile at 10 m from the pile axis was taken to couple the near and far fields using the NM expansion technique. The sound field predicted by the normal mode method at 130 m from the pile was converted into the waveform using inverse Fourier transform and then compared with the waveform predicted directly by FEM. The result is shown in Figure 2.10, which demonstrates that the prediction of the waveform in the far field via normal mode expansion is sufficiently accurate.

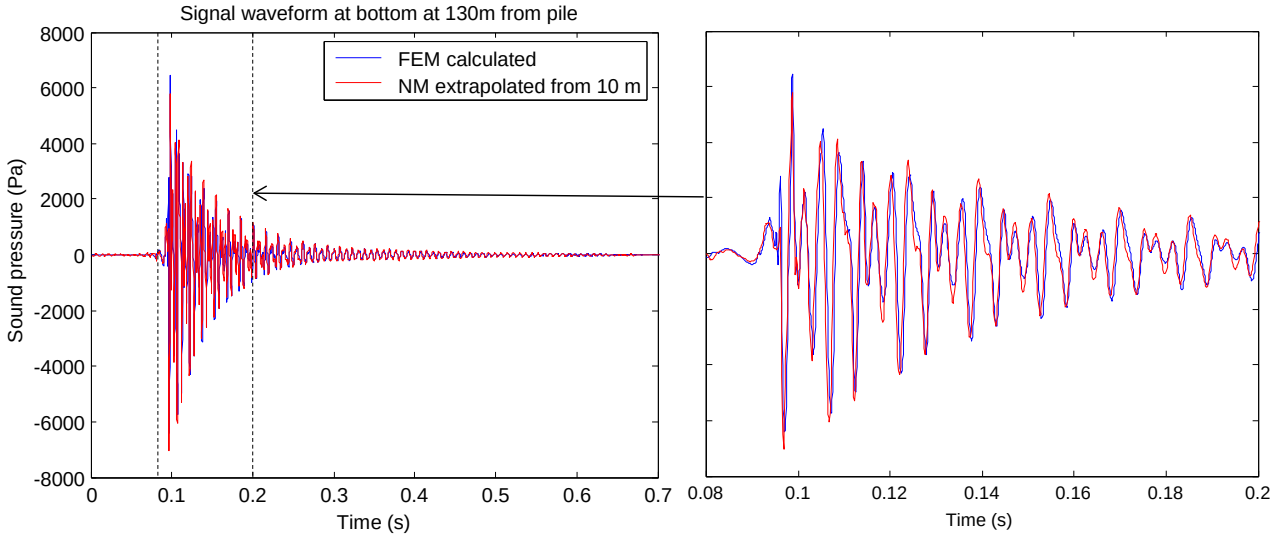


*Figure 2.10: Waveform of an underwater sound signal from a single blow numerically predicted at a distance of 130 m from the pile using direct FEM calculations (blue) and near-to-far field coupling method via NM expansion from the FEM solution at 10 m (red).*

During the near-field measurement program, only one noise logger (Logger #2 in Table 3.1) was in operation in the far field. The sea depth along the sound transmission path from the piling area to this logger varied significantly as a result of dredging around the turning basin. It was 13.5 m to 15 m in the area of bents 46 to 51, depending on tide phase, and 6.5-7.5 m at the logger location. An abrupt change in water depth took place at the edge of the dredging area, as can be seen on the bathymetry map in Figure 2.3. This is also illustrated in a model of the bathymetry profile along the transmission path (Figure 2.11) derived from the multibeam sonar data and bathymetry charts, which was used to numerically model the sound transmission. Such a significant change in bathymetry affects greatly the sound transmission loss, which will be demonstrated in Section 4.

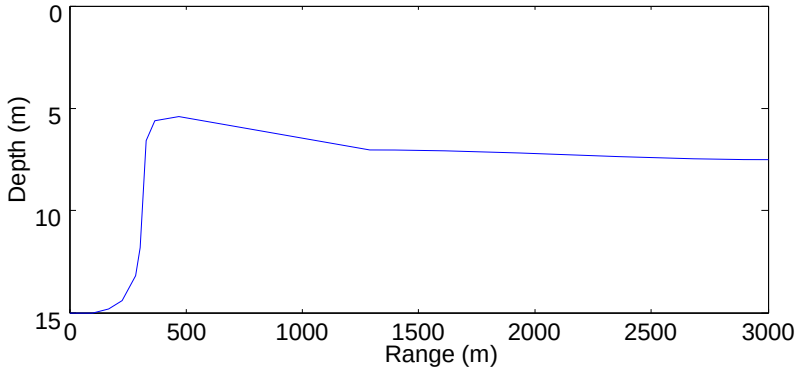


*Figure 2.11: Bathymetry from pile 51-2 to the far-field noise logger (#2 in Table 3.1)*

An adiabatic mode approximation method (Jensen *et al.*, 2011) was used to model the sound transmission in a range dependent underwater sound channel after coupling the near and far fields at 10 m from the pile. Sound attenuation in the sediment plays a noticeable role in the transmission loss of signals propagated over long distances in shallow water. Therefore it was included in the geoacoustic model of the seabed in the sound transmission model. Two values commonly accepted for sound attenuation in sand, $\gamma$ = 0.7 dB/$\lambda$ (Jensen *et al*., 2011) and $\gamma$ = 0.47 dB/$\lambda$ (Lippert *et al*., 2016) were tested.

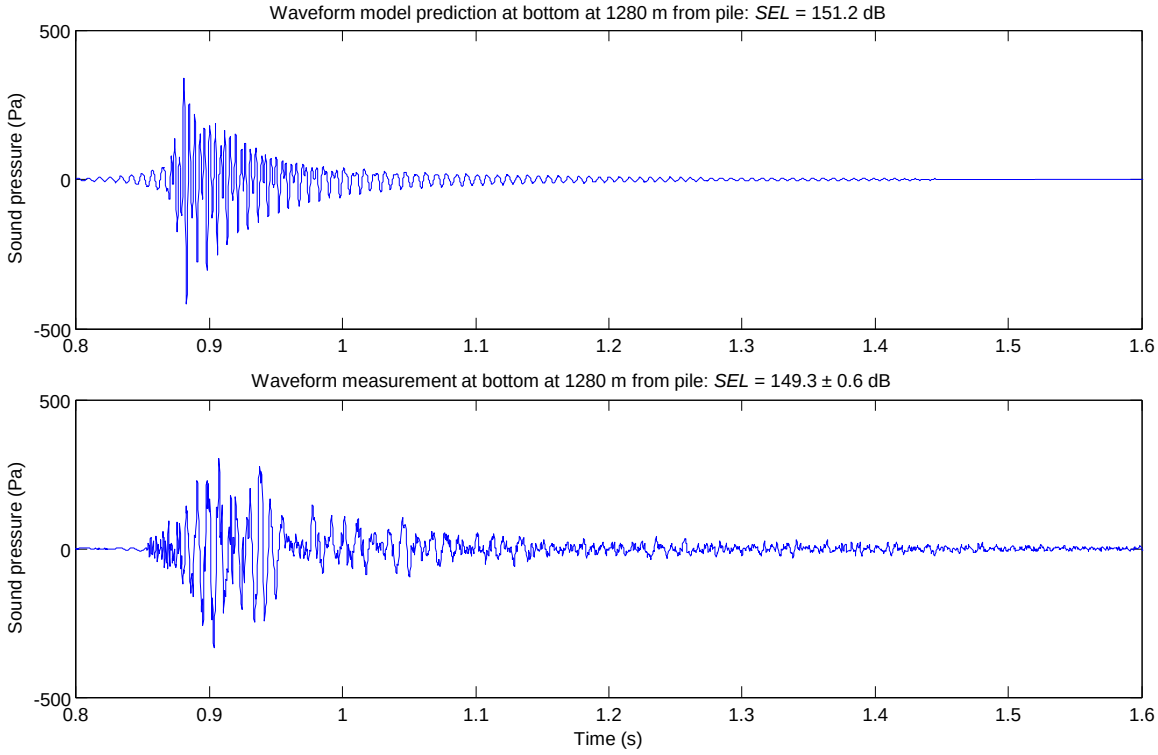


*Figure 2.12: Waveform of an underwater sound signal from a single blow modelled (top) and measured (bottom) at the bottom at a distance of 1280 m from pile 51-01.*

Figure 2.12 compares the waveform of sound signal recorded from one of strikes of pile 51-1 at about 1280 m (bottom panel) with the waveform modelled using: (1) FEM in the near field, (2) normal mode expansion approach for near-to-far field coupling, and (3) adiabatic mode method for modelling sound transmission in a range dependent underwater sound channel (top panel). Although the measured and modelled waveforms look somewhat different, the maximum amplitude of sound pressure, signal decay rate and energy are similar. The *SEL* values differ by approximately

2 dB, which is not much in terms of underwater sound transmission prediction. The difference in waveform details is not surprising, as the numerical model uses a simplified geoacoustic model of the seabed and does not take into account some likely effects of sound transmission, such as mode coupling and backscatter over a steep bottom slope at about 250 m and sound reflection from other underwater objects (e.g. other piles).

# 3. Long-term monitoring of underwater piling noise

## 3.1 Methodology

Four CMST-DSTO sea noise loggers (http://cmst.curtin.edu.au/products/usr.cfm) were deployed in the monitored area on the 8th of November 2014. The deployment locations are given in Table 3.1 and shown in Fig. 3.1. Unfortunately, the internal hydrophone contact in Logger #3 was damaged during deployment, so it did not make any sea noise recording. Also, after a heavy overnight storm on the 13th of March, the hydrophone of the most inshore Logger #1 partly lost its sensitivity, especially at higher frequencies, which was most likely due to a crack in its ceramic caused by wave impacts.

Logger #4 was recovered earlier, on the 9th of April, as the surface navigation buoy had detached from the mooring system. Loggers #2 and #4 were redeployed at the same locations on the 14th of March to continue sea noise recording until the 6th of August when they were finally retrieved. The timeline of all deployments is illustrated in Figure 3.2.

*Table 3.1: Coordinates of noise logger moorings (WGS 84 datum), distance to shore and water depth at mean sea level*

| Logger No. | Mooring location | Distance to shore (m) | Sea depth (m) |
|---|---|---|---|
| Noise Logger #1 | 21°40.195'S<br>115°0.133'E | ~1000 | ~6 |
| Noise Logger #2 | 21°39.924'S<br>115°0.133'E | ~1500 | ~6 |
| Noise Logger #3 | 21°39.518'S<br>115°0.133'E | ~2300 | ~7 |
| Noise Logger #4 | 21°39.112S<br>115°0.133'E | ~3000 | ~7 |

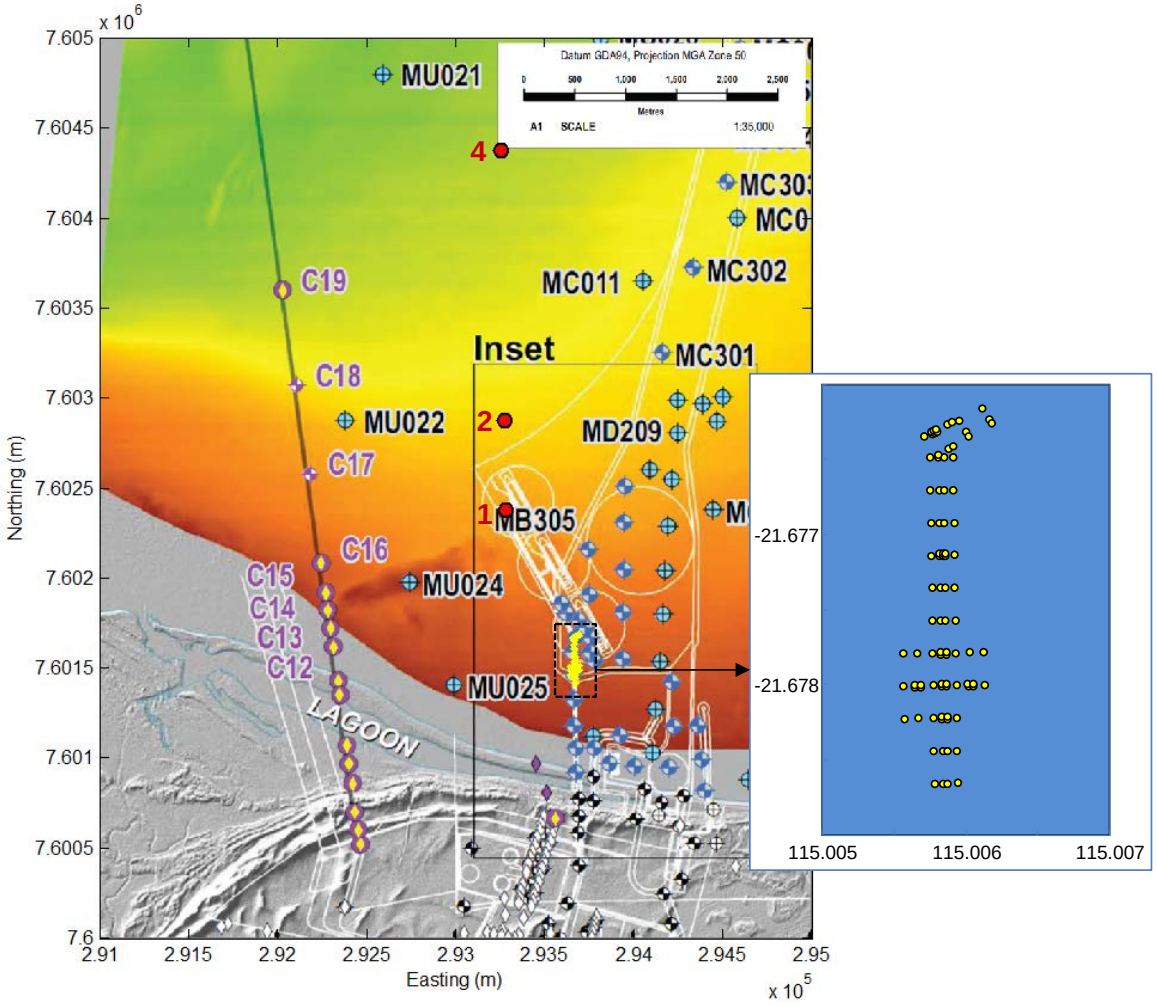


*Figure 3.1: Location of piles (yellow dots) and noise loggers (red dots) used to monitor underwater noise from impact pile driving during the construction of the Wheatstone jetty and berths. The small panel shows the layout of the piles from which underwater noise was recorded.*

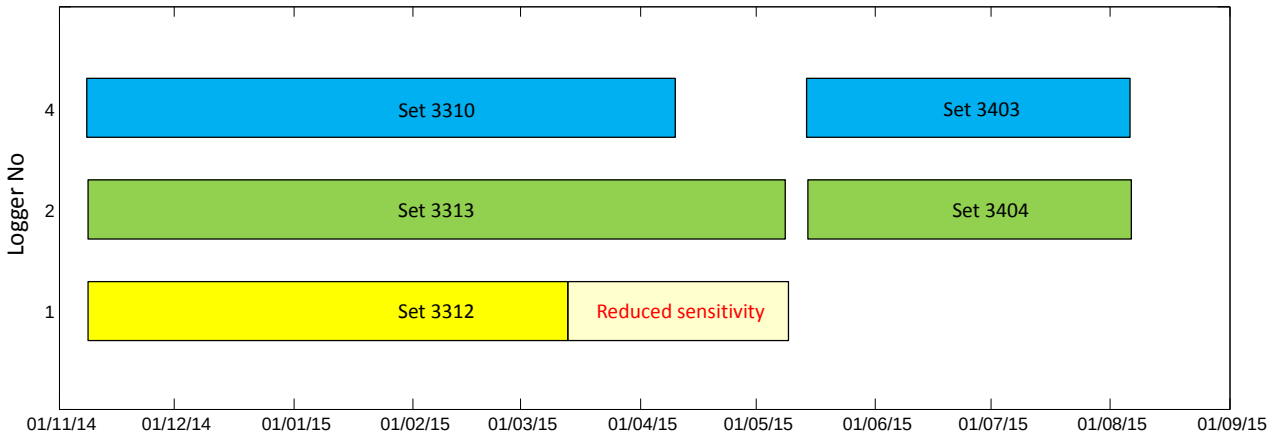


*Figure 3.2: Timeline of Wheatstone sea noise logger deployments from November 2014 to August 2015.*

The sea noise loggers used for the Wheatstone piling noise monitoring were designed and built at CMST. The housing of each logger was equipped with cross-bars, as shown in Figure 3.3, to stabilize its position on the seafloor. The loggers were deployed using moorings with surface buoys as outlined in Figure 3.4.

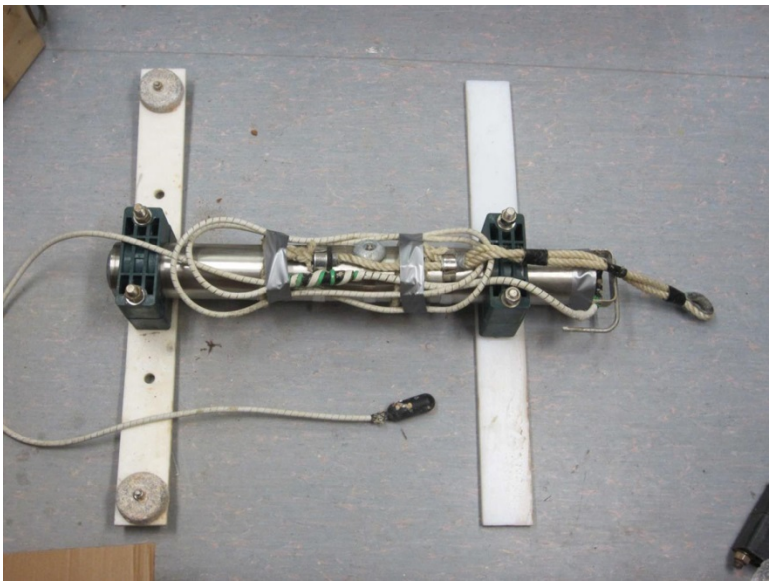

*Figure 3.3: Picture of the CMST sea noise logger mounted on two crossbars.*

The gain of an impedance matching pre-amplifier in the noise loggers was set at 20 dB. The underwater noise signal was digitized at a sampling rate of 8 kHz using a 16-bit analogue-to-digital converter. An anti-aliasing filter with a cut-off frequency of 3.8 kHz was applied to the analogue signal before conversion. All four loggers were programmed to make continuous 450 s long recordings with 900 s intervals between the recording start times. All noise loggers were calibrated before deployment by using a white noise signal of known level as an input signal of the recording system with the hydrophone connected in-series to the noise generator. The recorded signals and their spectra were corrected for the end-to-end frequency response of the recording system (Figure 3.5), so that the sound pressure and power spectrum density were measured in absolute units (µPa and µPa$^2$/Hz respectively).

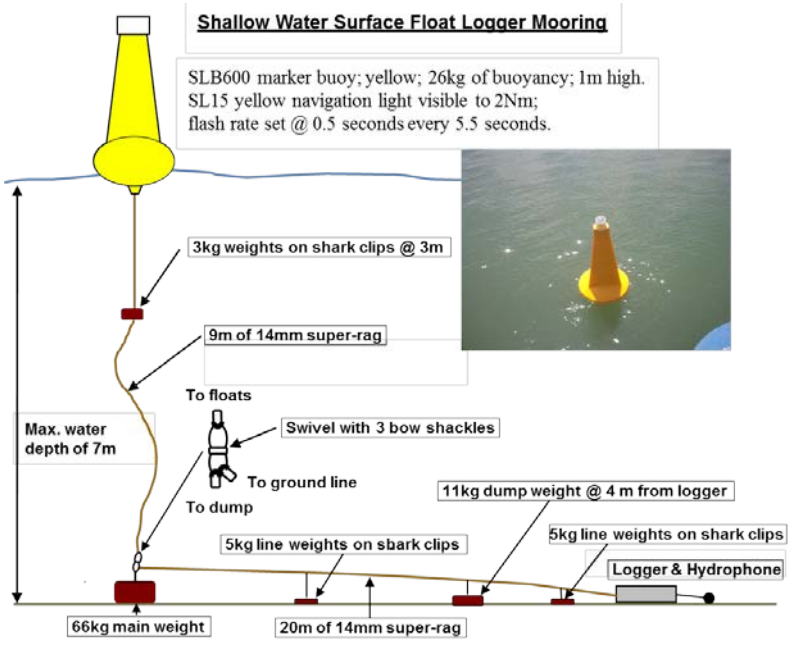


*Figure 3.4: Mooring schematic with noise logger.*

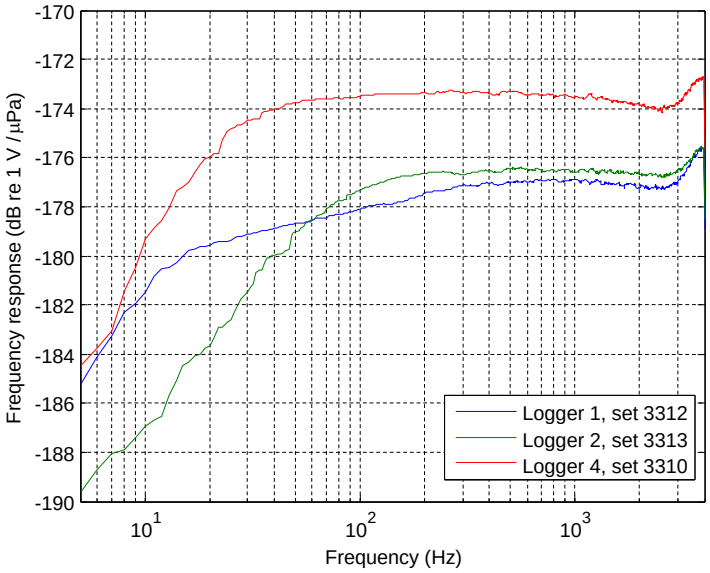


*Figure 3.5: Frequency response of the sound recording system of Loggers #1, #2 and #4.*

Underwater noise from a majority of the piles was recorded at all three locations at distances from about 900 m to nearly 3 km. Time periods containing from about 100 to 300 blows were selected from each pile, when the pile was driven in a regular (post soft-start) regime with a nearly uniform blow/hammer energy distribution. The hammer energy in the regular regime varied between different piles from about 200 kJ to nearly 300 kJ, with the majority of blows made with an interval of 270-290 kJ.

Two types of pile were driven to construct the jetty - vertical and slanting (rakers). Except piles PI-TR-44-6 and PI-TR-44-11, all vertical piles were 1016 mm in outer diameter with a wall thickness of 22 mm. The slanting piles and two larger vertical piles were 1200 mm in diameter with 25-mm walls. All slanting piles had a rake of 1:4, i.e. a slant of about 14° relative to the vertical. The total number of hammer blows taken for this analysis was nearly 30,000 including about 22,600 blows of slanting piles and 7,300 blows of vertical piles.

Processing and analysis of noise recordings to identify sources of underwater noise in the monitored area were performed using a Matlab software tool for the Characterisation of Recorded Underwater Sound (CHORUS) developed by the Centre for Marine Science and Technology at Curtin University (Gavrilov & Parsons, 2014). Figures 3.6 and 3.7 provide examples of underwater noise from various sources recorded by Loggers #2 and #4 over two different 10-day periods in November 2015 and February 2015. The top and middle panels in these figures show long-time average spectrograms of sea noise compiled from the Power Spectrum Density (PSD) measurements of each individual recording. These spectrograms reveal long-term changes in sea noise spectrum levels and allow of searching the major components in ambient noise in a time-efficient way. The multiple periods of intense continuous broadband noise from about 300 Hz to 2 kHz clearly seen in Figure 3.6 indicate the time of dredging operation in the Wheatstone turning basin and shipping channel. The periods of piling noise can be easily recognised, especially in set 3313, by broadband noise spanning frequencies form a few Hz to nearly 3 kHz. This ultralow frequency component of piling noise attenuated rapidly with range from driven piles and hence is hardly visible at the farthermost noise logger (top panel in Figure 3.6).

Three periods of pile driving can be distinguished during the 10-day period in February shown in Figure 3.7. Another source of intense underwater noise observed from February to May was a regular evening fish chorus that started after sunset and ended at around midnight. This chorus is

formed by overlapping pulsation sounds from many fishes of yet-unknown species, as shown in the bottom panel of Figure 3.7. It is important to notice that the intensity of sound from the fish chorus was on some days as high as that of the noise from piling at ranges less than 2 km.

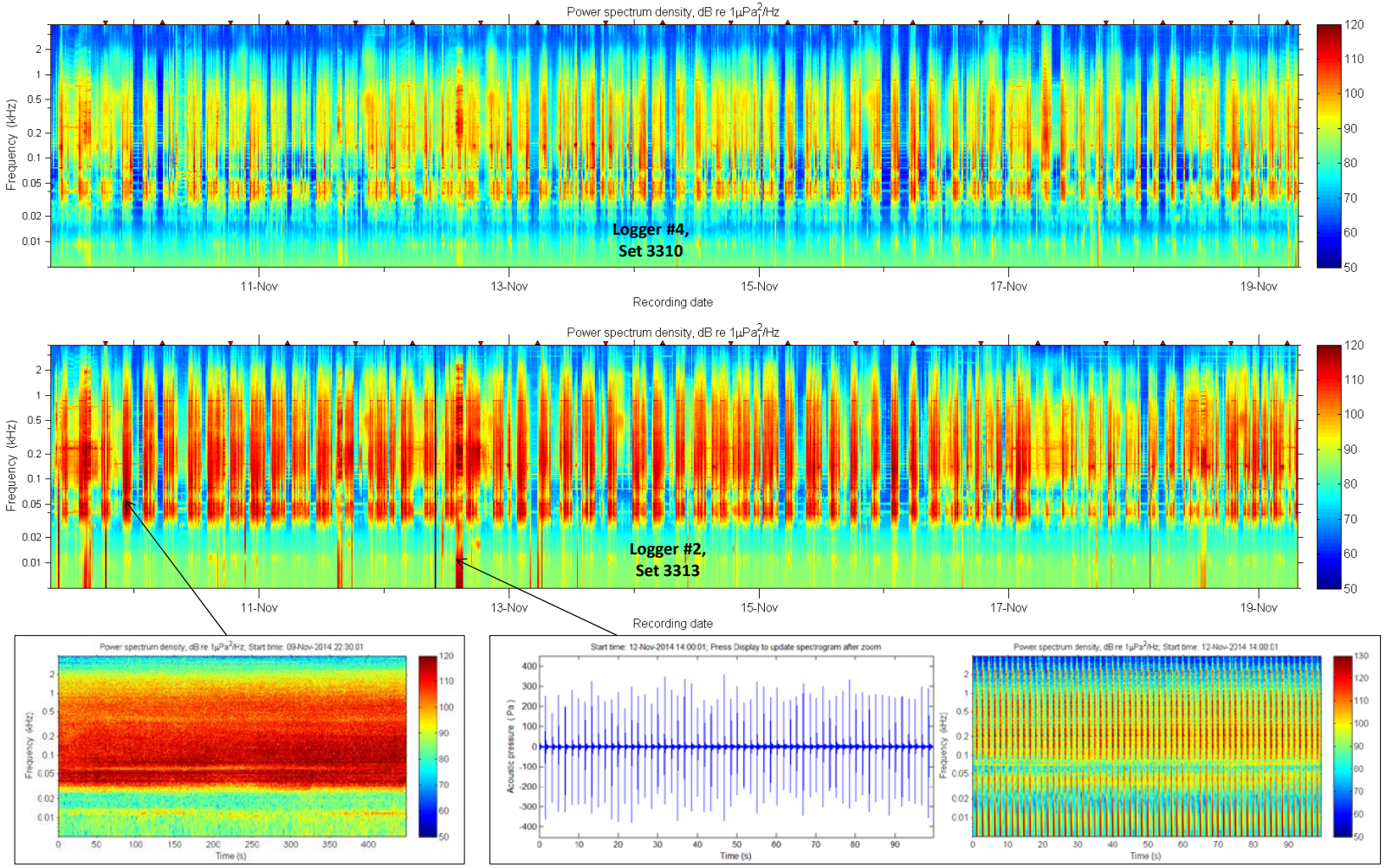


*Figure 3.6: Long-time average spectrograms of sea noise recorded by Loggers #4 (top panel) and #2 (middle panel) during 10 days in November 2014; typical spectrogram (from short-time Fourier transform) of dredging noise (bottom left); and waveform (bottom middle) and spectrogram (bottom right) of piling noise.*

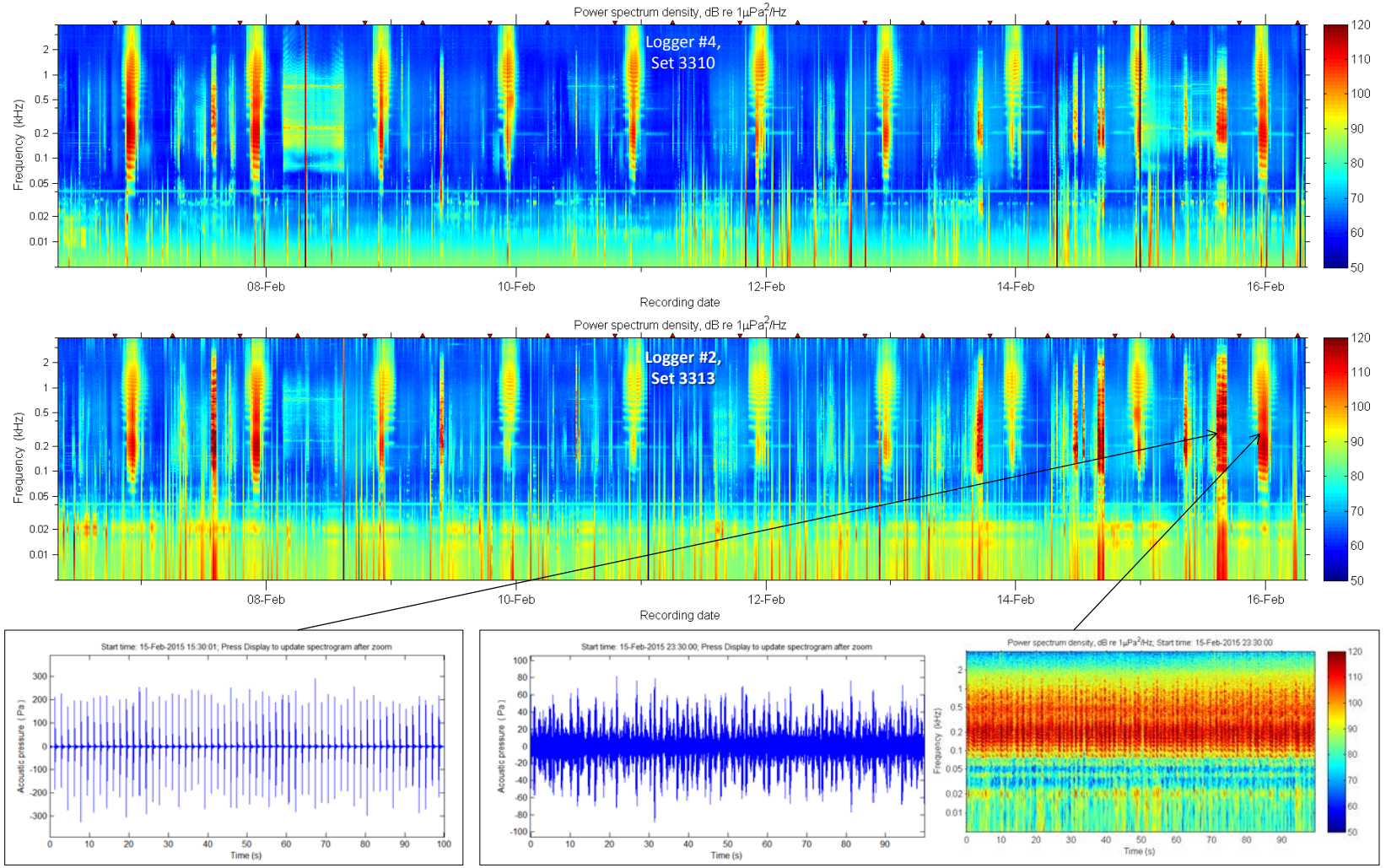


*Figure 3.7: Long-time average spectrograms of sea noise recorded by Loggers #4 (top panel) and #2 (middle panel) during 10 days in February 2015; waveform of piling noise (bottom left); and waveform (bottom middle) and spectrogram (bottom right) of noise from fish chorus.*

## 3.2 Library of sounds from underwater pile driving

To address item 10-17-i of WA Ministerial Statement No. 873 (Chevron, 2014), a library of sounds from the Wheatstone offshore piling operation has been compiled. It includes sounds recorded:

1) At different distances (item 10-17-i-a), as outlined in the previous section;
2) From piles of different size (item 10-17-i-b). Sounds from piles of different diameter and wall thickness were recorded, as well as from vertical and slanting piles. Sounds from piles of considerably larger size (diameter 1.7 m, wall thickness 45 mm) used to construct mooring dolphins, have not been recorded as the last dolphin pile was driven before the start of the noise monitoring program;
3) From two different piles driven concurrently at different distances (item 10-17-i-c). Only three events of concurrent piling were recorded and included in the library.

Items 10-17-i-d and 10-17-i-e related to different water depths and driving conditions/ bottom types respectively were difficult to address using the collected data. The water depth along the jetty section monitored for piling noise emission varied from about 13 m to nearly 16 m, which is insufficient to capture significant effects. The water depth at the receivers was also similar (Table 3.1).

Three boreholes (MT-308-310) were drilled along the jetty section and in the berth area monitored for piling noise. These three boreholes show that the substrate of more or less consolidated sediments (claystone, calcareous claystone and sandstone) were deposited from about 15 m to nearly 20 m below the seabed surface, overlaid with layered unconsolidated sediments, such as sand, clay and their mixture in various proportions with sparse gravel intrusions of various grain sizes. A review of pile installation records and new bathymetry data provided after dredging revealed that the total vertical penetration of the monitored piles into the ground was generally smaller than the depth of occurrence of consolidated sediments. Thus, the bottom type did not vary significantly between the piles.

For each recording of 100 to 300 blows selected as described in the previous section, the peak pressure level $SPL_{peak}$ = 10log(max{$p^2$}), sound exposure level $SEL = 10\log\left(\int_0^T p^2 dt\right)$ and RMS sound pressure level $SPL_{RMS}$ were measured for each blow and then their mean values and standard deviation were calculated. For impulsive noise signals, $SPL_{RMS}$ is not an adequate measure to assess potential impacts on marine fauna, as it varies rapidly with time. Moreover, there is no standard definition of how it should be measured in impulsive noises. However, as $SPL_{RMS}$ is currently the only accepted criterion to assess the effect of potential behavioural disturbance from underwater noise on marine mammals (Southall et al., 2007), here we define the RMS sound pressure level of a piling signal as $SPL_{RMS} = 10\log\left(\frac{1}{T}\int_0^T p^2 dt\right)$, where $T$ is the signal duration containing 90% of signal energy. This means that $SPL_{RMS}$ is calculated by averaging of $p^2$ over the signal duration.

The mean values and standard deviation were recorded in a spreadsheet (All piles processed data.xlsx) along with the distance to the sound receivers, pile ID and parameters, and hammer energy.

Also most representative fragments of 60 seconds length were manually selected form each recording to (1) save them in WAV files and (2) plot the calibrated waveform and save it in TIFF

files. Each WAV file is supplemented with a .CLB file of the same name which provides a calibration factor to convert the dimensionless amplitude in the WAV files into Pa. The spreadsheet and all WAV, TIF and CLB files are provided as supplement material to the report.

## 3.3 Correlation between peak pressure and sound exposure levels

### *Foreword*

Several studies, e.g. Gavrilov *et al*. (2007) and Galindo Romero *et al*. (2015), have shown that the peak pressure of impulsive noise signals propagated in the ocean cannot be accurately predicted at large distances by numerical models; in contrast to the signal energy and consequently sound exposure level that can be satisfactorily predicted, if basic environmental parameters are known. The major cause of this is that the instantaneous pressure of an acoustic signal and its maximum value in particular are subject to strong effects of constructive or destructive interference of signals propagated along different paths in the ocean sound channel. The interference effects in turn are sensitive to relatively small variations in the environment, which are impossible to accurately predict and model in a numerical model of underwater sound propagation in most of realistic scenarios. These variations include sea surface and bottom roughness and water-column inhomogeneities, which vary along the acoustic path and with time, and are commonly described by statistical models. Consequently, it would be logical to make predictions of the peak pressure using a statistical approach, i.e. its most expected value and possible variations around it.

Duncan *et al*. (2010) found a strong linear relationship between the peak-to-peak sound pressure level $SPL_{p\text{-}p}$ and the sound exposure level *SEL* of impulsive noise signals from marine impact pile driving in Port Phillip Bay, Victoria, Australia. The regression equation for $SPL_{p\text{-}p}$ derived from measurement data was:

$$SPL_{p\text{-}p} = A \times SEL + B, \quad (3.1)$$

where the regression coefficients $A$ and $B$ are the slope and offset respectively. All measured $SPL_{p\text{-}p}$ values lay within ±3dB around the levels predicted from the corresponding *SEL* by Eq. 3.1 with the regression coefficients $A$ = 1.12 and $B$ = 12.3 dB. Equation 3.1 can be modified for the zero-to peak sound pressure level $SPL_{peak}$ by reducing the offset coefficient $B$ by 6 dB, as the amplitude of positive and negative peak pressure values in impulsive sound signals are typically similar at distances much larger than the water depth. Therefore Eq. 3.1 for the Port Phillip Bay data can be rewritten as follows: $SPL_{peak} \approx 1.12 \times SEL + 6.3$ dB.

As both *SEL* and $SPL_{peak}$ are governed by the transmission losses increasing with range, the slope $A$ reveals the difference in the decay rate with range of these two measures. Slope coefficients $A > 1$ indicate that $SPL_{peak}$ decays with range faster than *SEL*. As shown in Lippert *et al.* (2015) and Galindo Romero *et al*. (2015) and will be discussed later in this section, the offset coefficient is governed primarily by sound source characteristics.

The finding of a linear relationship between *SEL* and $SPL_{peak}$ also suggested that numerical predictions of *SEL* could be used to predict $SPL_{peak}$ and its variations. Such a modelling approach has been effectively implemented for airgun signals from offshore seismic surveys (Galindo Romero *et al*., 2015) and for signals from underwater impact pile driving (Lippert *et al*., 2015).

### *Correlation analysis*

Figure 3.8 shows measurement results for $SPL_{peak}$ versus *SEL* for both vertical and slanting piles and the best linear fit of their dependence (Eq. 3.1) calculated using all 30,000 samples. The best fit resulted in regression coefficients $A$ = 1.132±0.002 and $B$ = 2.4±0.3 dB ($R^2$ statistic value of about 0.975 and *t*-statistics *p*-values less than $1 \cdot 10^{-50}$ at $n$ = 29167 degrees of freedom). The best fit calculated separately for the measurement data from vertical and slanting piles resulted in similar

coefficients: $A \approx 1.11$ and $B \approx 5.2$ dB for vertical piles and $A \approx 1.14$ and $B \approx 1.6$ dB for slanting piles.

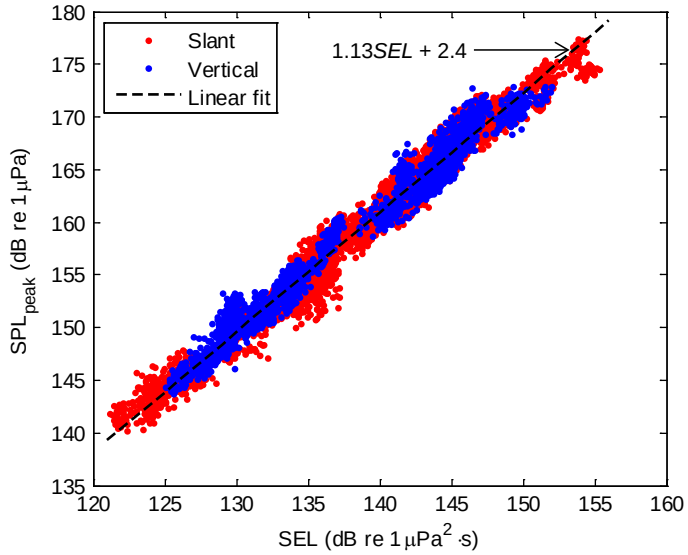


*Figure 3.8: $SPL_{peak}$ versus SEL measured from vertical (blue dots) and slanting (red dots) pile. The black dashed line shows the best linear fit for the relationship derived from all samples.*

Figure 3.9 shows the distribution of the difference between the measured $SPL_{peak}$ values and their prediction from the corresponding *SEL* values using Eq. 3.1 with the regression coefficients $A = 1.13$ and $B = 2.4$ dB. A normal distribution fit is also shown in the plot. The standard deviation $\sigma$ of the normal distribution fit is about 1.39 dB, which means that ~95% of measured $SPL_{peak}$ values are expected within an interval of ±2.8 dB around the prediction made by Eq. 3.1.

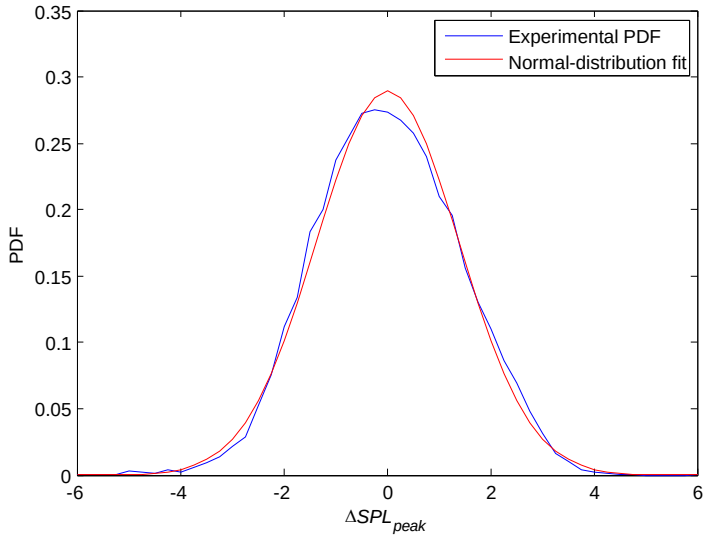


*Figure 3.9: Histogram of the difference between measured $SPL_{peak}$ values and their prediction from the corresponding SEL values using Eq. 3.1 with the regression coefficients A = 1.13 and B = 2.4dB (blue bars). The red line shows the normal distribution fit resulting in the mean at approximately 0 ($-2.4\times10^{-12}$) and standard deviation of about 1.39.*

It is important to notice that the slope $A = 1.13$ of the regression line (Eq. 3.1) derived from the Wheatstone piling noise measurements is similar to that measured in Port Phillip Bay. However, the

offset coefficient is somewhat different: $B$ = 2.4 dB in Wheatstone versus $B$ = 6.3 dB in Port Phillip Bay.

According to Lippert *et al.* (2015) and Galindo Romero *et al*. (2015), the difference in the offset $B$ can be driven by the sound source characteristics. The piles driven in Port Phillip Bay were 0.71 m in diameter with a wall thickness of 21 mm. They were driven by an IHC S90 hydrohammer with a 4.5-ton ram weight. Most of the Wheatstone piles were driven by an IHC S280 hydrohammer with a 13.6-ton ram. To correct for this difference, let us follow the approach implemented by Lippert *et al*. (2015) with some modifications. Assuming the basic model of hammer interaction with the pile head without cushioning (or damping in the pile and ram material), the force function applied to the pile head due to a hammer impact can be modelled as a function of time $t$ as follows (Deeks and Randolph, 1993):

$$f_p = Z_p V_r \exp\left[-\left(Z_p / M_r\right) t\right] , \tag{3.2}$$

where $Z_p = EA/C_p$ is the pile mechanical impedance, $E$ is Young's modulus of the pile material, $A$ is the pile's cross-section area, $C_p$ is the axial wave velocity in the pile, which is slightly lower than the compressional wave speed in the pile material (see Section 2.1 of this report), $V_r$ is the ram velocity at impact, and $M_r$ is the ram mass. The radial displacement of the pile wall and consequently the acoustic pressure in the radiated sound are proportional to the force function $f_p$, so that the peak pressure can be expressed as:

$$P_p = K_1 Z_p V_r , \tag{3.3}$$

where the coefficient $K_1$ allows for all effects resulting in impact-to-sound conversion.

The energy $E_S$ of a sound signal (or sound exposure) received at a certain distance from the pile is expected to be proportional to the sound energy radiated by the pile into the water column, which in turn is proportional to the impact energy $E_r = M_r V_r^2 / 2$, so the sound exposure $E_S$ can be expressed as:

$$E_S = K_2 M_r V_r^2 / 2 , \tag{3.4}$$

where the coefficient $K_2$ allows for energy losses due to pile-ground friction, sound radiation into the seabed and spreading loss in the underwater sound channel.

Eqs. 3.3 and 3.4 can be used to calculate the expected difference between $SPL_{peak}$ and $SEL$:

$$SPL_{peak} - SEL \equiv 20\log P_p - 10\log E_S = 10\log\left(\frac{Z_p^2}{M_r}\right) + 10\log\left(\frac{K_1}{K_2}\right) + 3. \tag{3.5}$$

Notice that this difference does not depend on impact energy.

Let us assume now that the regression coefficients $A_0$ and $B_0$ were derived from a reference dataset measured for certain pile and hammer types with parameters $Z_{p0}$ and $M_{r0}$. Let us also assume that changes in the piling and environmental characteristics do not significantly affect the ratio of coefficients $K_1$ and $K_2$. In this case, the regression formula derived from the reference measurements can be used to predict $SPL_{peak}$ from $SEL$ for other pile and hammer parameters using a correction term based on Eq. 3.5:

$$SPL_{peak} = A_0 \times SEL + B_0 + 10\log\left(\frac{Z_{p0}^2 M_r}{Z_p^2 M_{r0}}\right). \tag{3.6}$$

If the Wheatstone data are used as a reference set, then the correction of $B$ for the Port Phillip Bay dataset is -1.4 dB, i.e. $B$ = 6.3 – 1.4 = 4.9 dB, which is still higher than the best fit value $B$ = 2.4±0.3 dB derived from the Wheatstone data. However, the difference is only about 2 dB.

Thus Eq. 3.6 can be used to predict mean $SPL_{peak}$ values from either measured or modelled $SEL$ values for different piles and hammers. The probability of $SPL_{peak}$ to be below a certain threshold can be estimated using an empirical, nearly normal distribution of fluctuations around the mean shown in Figure 3.9. A comparison of empirical predictions for $SPL_{peak}$, using numerical predictions for $SEL$ and Eqs. 3.1or 3.6, with experimental data is beyond the scope of this study.

### *Theoretical foundation for the distribution of $SPL_{peak}$ fluctuations*

Analysis of experimental data shows that fluctuations of $SPL_{peak}$ around its predicted value can be reasonably well approximated by a normal distribution, as shown in Figure 3.9. However, a theoretical foundation can also be suggested to model the distribution function of $SPL_{peak}$ variations. Let us consider the case of an underwater sound signal arriving at a receiver via a large number of different paths in the ocean sound channel with a random phase relationship due to various scattering effects, which is a typical scenario at large distances from the signal source. If the scattered (incoherent) component is large compared to the coherent one, than the instantaneous sound pressure $p$ will tend to be normally distributed (Dyer, 1970), its magnitude $|p|$ Rayleigh distributed and its squared value $|p|^2$ exponentially distributed.

Let us now consider a series of signals either selected from statistically independent sections of a continuous signal or constructed from a series of impulsive signals received at the same location but at sufficiently different times. If the squared amplitude $|p|^2$ in each of these signals is exponentially distributed with approximately the same mean value, then the maximum $|p|^2$ values, $\max\{p^2\}$, taken from all signals in the series will tend to be extreme value (Gumbel) distributed (Beirlant, 2004). The generalized Gumbel distribution has the cumulative distribution function

$$F(x,\alpha,\beta) = \exp\left[-\exp\left(\frac{\beta - x}{\alpha}\right)\right],$$

where $\alpha$ and $\beta$ are the scale and location parameters respectively. The quantile function of Gumbel distribution is:

$$Q(p) = \beta - \alpha \ln[-\ln(p)], \qquad (3.7)$$

where $P$ is probability.

This theoretical foundation for the statistics of $p_{peak}^2 = \max\{p^2\}$ could be verified by the Wheatstone experimental data, if the mean value of $p^2$ was similar for all signals recorded during measurements. However, the measurements were made at significantly different distances from driven piles and at different energy of hammer strikes, so the received sound pressure $p$ varied significantly due to different transmission losses and source levels. To surmount this problem, one can use the linear relationship between $SPL_{peak}$ and $SEL$ given by Eq. 3.1. Simple transformation of Eq. 3.1 results in:

$$\frac{p_{peak}^2}{E_S^A} = 10^{B/10}, \qquad (3.8)$$

where $p_{peak}$ is the peak pressure of piling signals and $E_S = \int_0^T P^2 dt$ is the sound exposure. Equation 3.8 shows that the mean value of $\frac{p_{peak}^2}{E_S^A}$ should remain constant, regardless the source distance and level, and all variations of $p_{peak}^2$ should result in fluctuations of $\frac{p_{peak}^2}{E_S^A}$ around its mean value.

Figure 3.10 shows the experimental probability density function of $\frac{p_{peak}^2}{E_S^A}$ derived from all 30,000 piling signals used for analysis and its best fit by a Gumbel distribution. As one can see, the approximation of the experimental distribution by the Gumbel model is reasonably accurate. The mean of the Gumbel model distribution is $\beta + \gamma\alpha = 1.84$, where $\gamma \approx 0.577$ is the Euler-Mascheroni constant, which is close to $10^{B/10} = 1.75$ expected from Eq. 3.8.

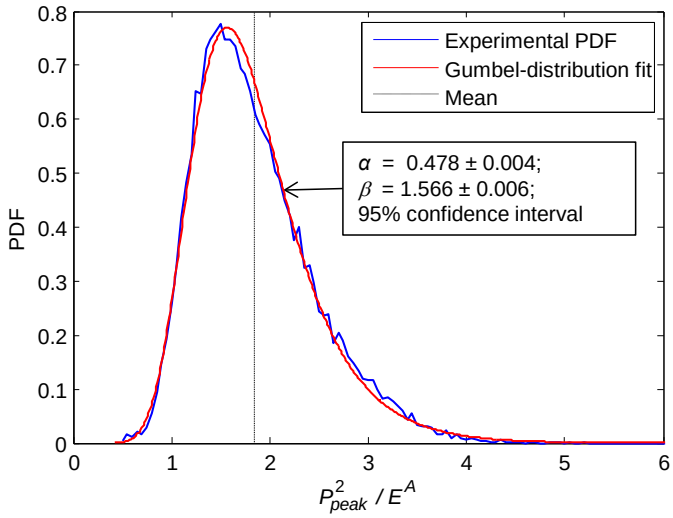


*Figure 3.10: experimental distribution of $\frac{p_{peak}^2}{E_S^A}$ (blue) and its best fit by a Gumbel distribution (red). The black dashed line show the mean of the Gumbel model distribution.*

A closed-form expression is not available for the distribution functions of a logarithm of a Gumbel-distributed variable. However, numerical simulations show that the probability density function (PDF) of such a random variable looks similar to a normal distribution within a reasonable range of variation of the parameters $\beta$ and $\alpha$. In Figure 3.10 a numerically simulated PDF (normalised histogram) of function $y = 10\log(x)$, where $x$ is a Gumbel-distributed variable with $\alpha = 0.48$ and $\beta = 1.57$, is compared with its best fit by a normal distribution. As one can see, the normal distribution models quite well the numerically simulated distribution of $y$. At other values of $\alpha$ varying from 0.25 to 1.5 and $\beta$ from 1 to 5, the similarity is good enough to use the normal distribution for estimating the probability of $SPL_{peak}$ values.

### *Algorithm to predict the probability of $SPL_{peak}$*

As the peak pressure level of an impulsive signal propagated in a varying ocean sound channel is in essence a stochastic characteristic, its prediction should be based on a statistical approach. In most applications, it is important to predict a threshold value below which the $SPL_{peak}$ value is expected to fall with a certain probability (or for a certain percentage of time). Based on the results given in the previous sections, the following algorithm can be suggested:

1. The combined offset $B$ in Eq. 3.6 is estimated using the reference offset $B_0$ and the correction term that allows for differences in the actual and reference characteristics of piles and hammers;
2. The location parameter of the Gumbel distribution, $\beta = 10^{B/10} - \gamma\alpha$ is calculated, assuming the scale parameter $\alpha \approx 0.5$ to be similar for different measurements;
3. The probability $P$ is chosen and then the threshold $\left.\frac{p_{peak}^2}{E_S^A}\right|_P$ is calculated using the quantile function (Eq. 3.9);
4. Using the empirically derived coefficient $A = 1.13$ and either measured or numerically predicted values of the sound exposure $E_S$, the threshold for peak pressure and its level are calculated, so that $p\times100\%$ of signals are expected to have $SPL_{peak}$ values below this threshold.

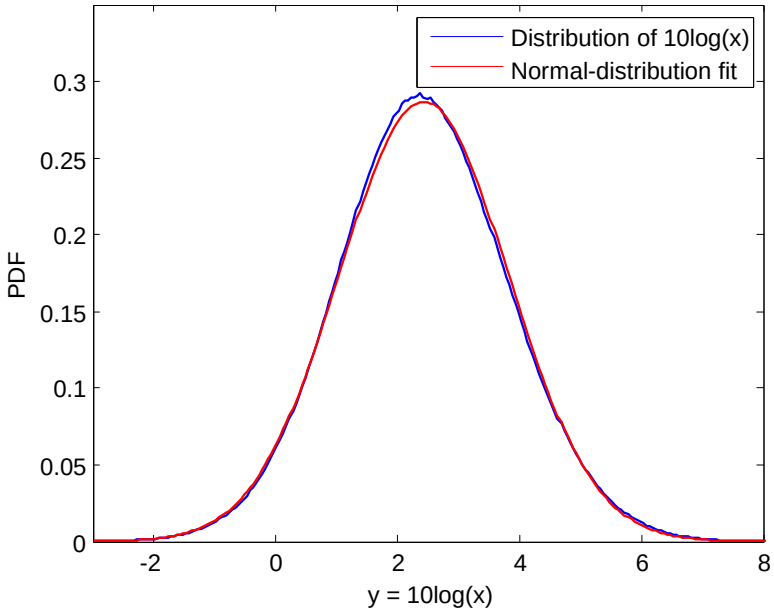


*Figure 3.11: Numerically simulated PDF of function y = 10log(x), where x is a Gumbel-distributed variable with α = 0.48 and β = 1.57 (blue bars) and its best fit by a normal distribution (red line).*

The algorithm suggested here needs to be thoroughly verified using data from different piling operations with different piles and hammers and in different environments, which is beyond the scope of this research project.

## 3.4 Difference in the sound level from vertical and slanting (raker) piles

Figures 3.12 and 3.13 show variations of the measured *SEL* values with range from the vertical and raker piles respectively. It is obvious from comparison of these two plots that the sound level from the raker piles driven at similar distances from the acoustic receiver varied much more than that from the vertical piles. The most reasonable explanation of such large variations in the noise level from the raker piles is that the aspect of their tilt relative to the sound transmission direction was different for different piles (see Figure 3.14 for illustration).

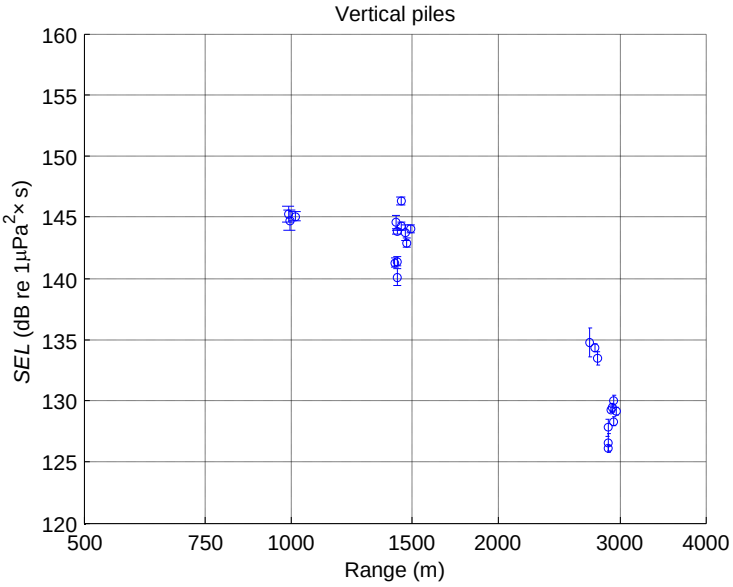


*Figure 3.12: Sound exposure level from the vertical piles measured by three noise logger at different distance from piles.*

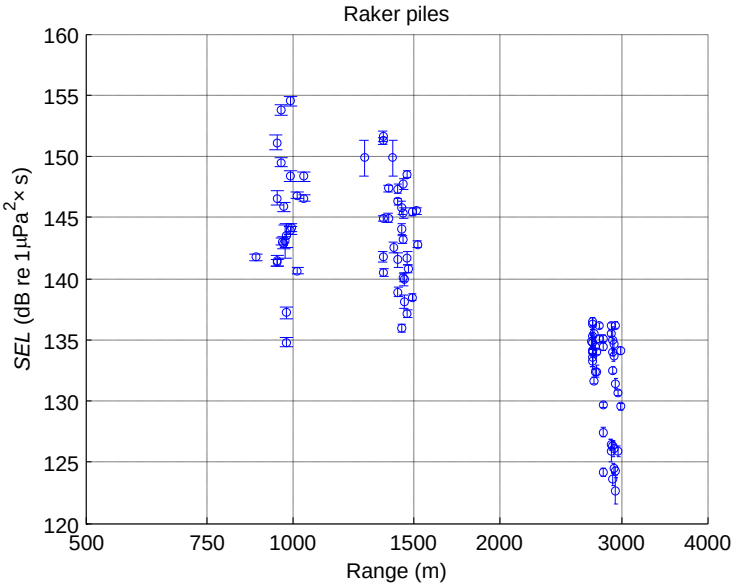


*Figure 3.13: Sound exposure level from the raker piles measured by three noise logger at different distance from piles.*

Although a numerical model of sound emission from slanting piles has not been developed yet due to computational difficulties (the problem is not axisymmetric anymore), it is obvious from general physical consideration that the sound emission in the direction of pile bearing should be different than that in the opposite direction.

As demonstrated in several publications (e.g. Reinhall & Dahl, 2011 and Wilkes & Gavrilov, 2016), an impact driven pile emits a wavefront similar to a Mach cone at an angle $\theta = \sin^{-1}\left(c_w / c_p\right)$ relative to the pile axis, where $c_w$ is the sound speed in water and $c_p$ is the longitudinal wave velocity of radial deformation in the driven pile. For the Wheatstone jetty piles, $c_p$ = 5420 m/s and $\theta \approx 16°$. The rake of all slanting piles was 1:4, i.e. about 14° relative to the vertical. This means that the sound wavefront from the pile was nearly vertical and hence propagated almost horizontally in the direction of pile bearing, in contrast to the opposite direction where it was radiated into the seafloor at a much steeper angle.

To examine this effect, the measured *SEL* values were plotted against azimuth angle of the transmission direction relative to pile bearing. To minimise the effect of range, measurements made only by Logger #2 at 1300-1500 m from the piling site were taken into consideration. The result is demonstrated in Figure 3.15. Although there are random-looking variations, the general trend is evident – the level of piling noise emitted in the direction of raker pile bearing (0°, see illustration in Figure 3.14) was 10 to 15 dB higher than that in the opposite direction (180°). As the regular (post soft start) hammer energy used to drive raker piles was similar (270-300 kJ), the major cause of random-like variations was most likely the difference in the seabed sediments at different pile locations.

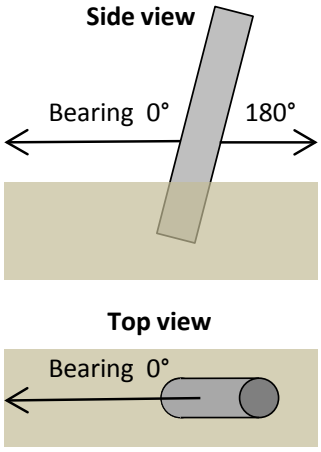


*Figure 3.14: Bearing angle of raker pile.*

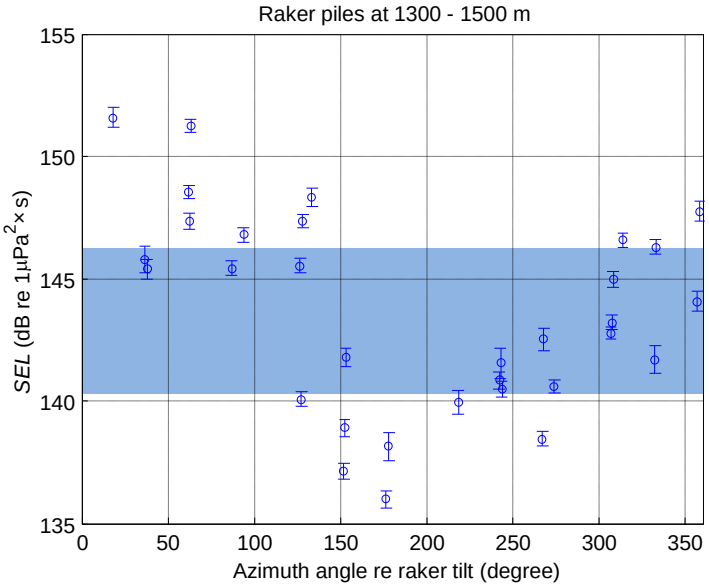


*Figure 3.14: Sound exposure level from the raker piles measured by noise Logger #2 versus azimuth angle of the transmission direction relative to pile bearing. Blue band shows the variation range of SEL from the vertical piles measured by the same noise logger.*

# 4. Assessment of potential impact of piling noise on marine fauna

## *Noise from single piles*

To assess potential impacts of man-made underwater noise on marine animals, it is needed to: (1) establish criteria of various potential impacts and (2) predict, via measurements or modelling, noise characteristics as a function of distance from the noise source. The sound exposure and peak pressure levels are commonly used as criteria to assess possible hearing injury and Temporal hearing Threshold Shift (TTS) in marine animals due to impulsive noise. The RMS sound pressure level is used as a criterion for continuous noise.

According to data from several visual and acoustical surveys, humpback whales, dolphins and green turtles are the marine animal species of interest with respect to potential impacts of man-made underwater noise from Wheatstone offshore operations, as these animals reside in the surrounding coastal area on either a permanent or seasonal basis. There is very little information in the available literature about the thresholds for the sound exposure level *SEL*, the peak pressure level $SPL_{peak}$ and the RMS sound pressure level $SPL_{RMS}$ affecting humpback whales, dolphins and turtles. The values used in the SVT reports (Chevron, 2011, vol.2 and vol.3) and in this study were taken from Southall et al, 2007 and Popper *et al.*, 2006. They are summarised in Tables 4.1 and 4.2.

*Table 4.1: Threshold levels of $SPL_{peak}$, $SPL_{RMS}$ and SEL, above which physical injury, TTS onset or behavioural disturbance may take place for humpback whales and dolphins (based on Southall et al., 2007)*

| Metric | Possible physical injury | | Possible onset of TTS | | Possible behavioural disturbance | |
|---|---|---|---|---|---|---|
| | Humpback whales | Dolphins & dugongs | Humpback whales | Dolphins & dugongs | Humpback whales | Dolphins & dugongs |
| $SPL_{peak}$ (dB re 1µPa) | 230 | 230 | No data | No data | No data | No data |
| $SPL_{RMS}$ (dB re 1µPa) | No data | No data | No data | No data | 120 | 120 |
| *SEL* (dB re 1µPa$^2$·s) | 198 | 198 | 183 | 183 | No data | No data |

*Table 4.2: Threshold levels of $SPL_{peak}$, $SPL_{RMS}$ and SEL, above which physical injury or behavioural disturbance may take place for turtles (based on Popper et al., 2006).*

| Metric | Possible physical injury | | Possible behavioural disturbance | |
|---|---|---|---|---|
| | Adult turtles | Turtle hatchlings | Adult turtles | Turtle hatchlings |
| $SPL_{peak}$ (dB re 1µPa) | 222 | 208 | No data | No data - |
| *SPL RMS* (dB re 1µPa) | No data | No data | 175 | No data |
| *SEL* (dB re 1µPa$^2$·s) | No data | 187 | No data | No data |

Because the measurements of underwater piling noise were made at sparsely distributed distances from the piles (see Figures 3.12 and 3.13), the major characteristics of sounds signals, *SEL*, $SPL_{peak}$ and $SPL_{RMS}$ were calculated as a function of distance from the pile using the numerical model discussed in Section 2 and validated by measurements at some reference distances. These characteristics were calculated for a vertical pile of 1016 mm in diameter (pile 51-01) driven with hammer energy of 198 kJ. Correction for different hammer energy is straightforward as the energy (and squared pressure) of sound emitted in water is proportional to hammer energy in the model; e.g. for a hammer energy of 280 dB, all modelled characteristics should be increased be approximately 1.5 dB regardless the distance. Correction for the difference between the vertical and raker piles is less straightforward. It can be made based only on the measurements of different piles at similar distances, such as those shown in Figure 3.15. According to these measurements, the sound pressure level of signals received from the raker piles at azimuth angles of around 0° relative to the pile bearing was 5 to 8 dB higher than the mean level from the vertical piles at similar distances. So, for raker piles driven at hammer energy of 280 kJ, the maximum (conservative) correction for the *SEL* would be 9.5 dB. Similar corrections were also assumed for $SPL_{peak}$ and $SPL_{RMS}$ for the raker piles.

It is not certain how the RMS sound pressure level $SPL_{RMS}$ should be defined for impulsive noise to apply it as a criterion of possible behavioural disturbance based on the data presented in Tables 4.1 and 4.2. It's also not fully clear, how this level was defined in the SVT reports (Chevron, 2011, vol.2 and vol.3). Based on the information provided in these reports, sound levels were modelled in the frequency domain and then integrated over the modelled frequency band; hence $SPL_{RMS}$ was estimated for continuous noise. To make estimates more physically reasonable, we measured and calculated $SPL_{RMS}$ for the RMS sound pressure averaged only over the signal duration *T* containing

90% of its energy; thus, it relates to *SEL* as $SPL_{RMS} = SEL - 10\log T$ . The signal duration $T$ was about 0.3 s at the far-field loggers (see Figure 2.12 as an example). At a driving rate of 40 blows per minute, the time intervals containing piling signals account for only 20% of time. So, if RMS sound pressure level was measured using averaging over the duration of multiple strikes, then the $SPL_{RMS}$ would be about 7 dB lower.

Figures 4.1, 4.2 and 4.3 show *SEL*, $SPL_{peak}$ and $SPL_{RMS}$ respectively as a function of range numerically predicted using the modelling approach described in Section 2. The green lines demonstrate results obtained for the range dependent bathymetry shown in Figure 2.11. The blue lines demonstrating modelling results for a flat bottom of 15 m water depth are shown for comparison. The solid lines correspond to sound attenuation in the bottom of 0.7 dB/λ, while the dashed ones to that of 0.47 dB/λ. The red dots show results of measurements made from pile 51-01 at three reference distances in the near and far fields. As one can see, the numerical results based on the real bathymetry model predict quite accurately the measured levels – the difference is less than 1 dB.

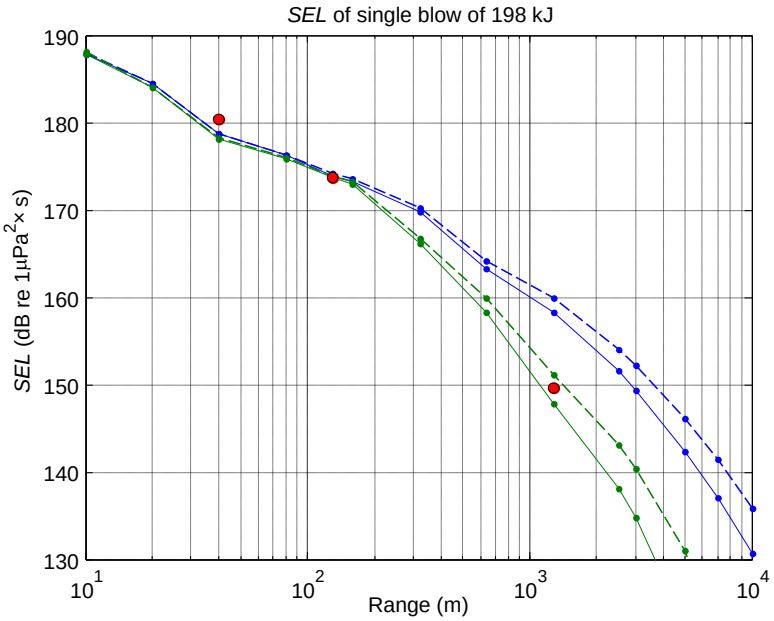


*Figure 4.1: Sound exposure level vs range modelled for constant sea depth of 15 m (blue lines) and range dependent bathymetry (green lines), as shown in Fig.2.11, (green lines) for sound attenuation in the sediment of 0.7 dB/λ (solid) and 0.47 dB/λ (dashed). Red dots show the mean values of measurement data for pile 51-1.*

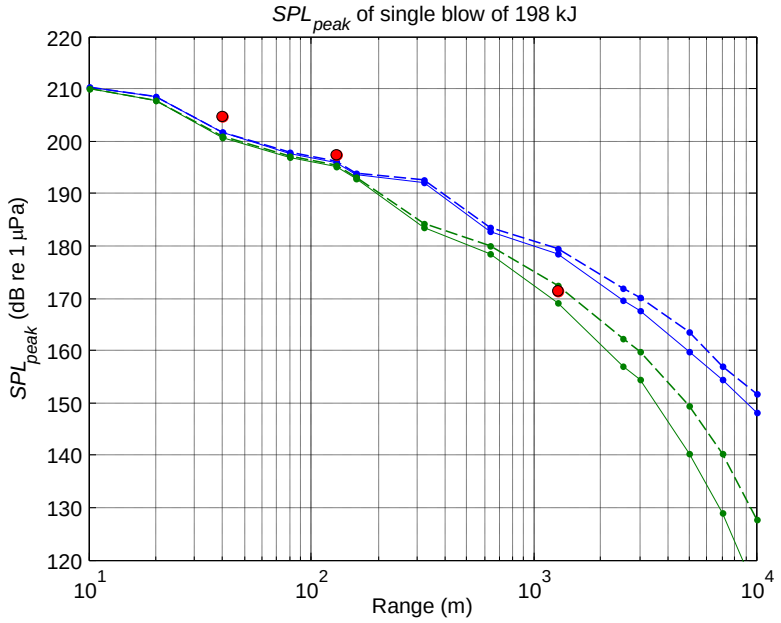


*Figure 4.2: Peak pressure level vs range modelled for constant sea depth of 15 m (blue lines) and range dependent bathymetry, as shown in Fig.2.11, (green lines) for sound attenuation in the sediment of 0.7 dB/λ (solid) and 0.47 dB/λ (dashed). Red dots show the mean values of measurement data for pile 51-1.*

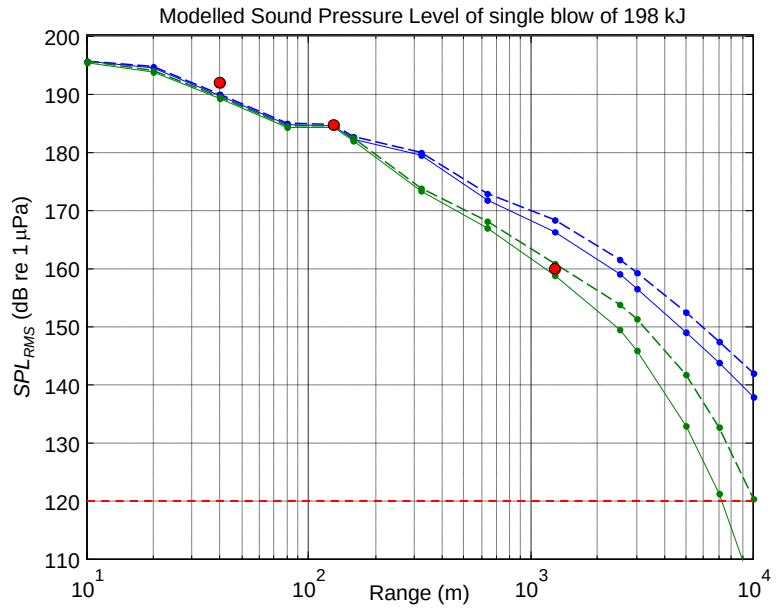


*Figure 4.3:Mean sound pressure level of piling signals vs range modelled for constant sea depth of 15 m (blue lines) and range dependent bathymetry shown in Fig.2.11 (green lines) for sound attenuation in the sediment of 0.7 dB/λ (solid) and 0.47 dB/λ (dashed). Red dots show the mean values of measurement data for pile 51-1. Red dashed line shows the level of potential behavioural disturbance of humpback whales and dolphins.*

It follows from Figure 4.2 that the peak pressure levels were low enough to eliminate any possibility of physical injury of hearing to humpback whales and dolphins at distances beyond 10 m from the pile.

As regular driving of individual piles for the Wheatstone jetty never lasted longer than 1 hour, the cumulative *SEL* was calculated for continuous driving duration of 10 min,

30 min and 1 hour, assuming the average strike rate of 40 blows per minute, which was close to the highest rate of regular driving at any time. The numerical predictions of the cumulative *SEL* versus range calculated for 10 min, 30 min and 1 hour time periods are shown in Figures 4.4, 4.5 and 4.6 respectively. The threshold levels of physical injury and TTS onsets for humpback whales and dolphins are also shown on these plots by dashed horizontal lines.

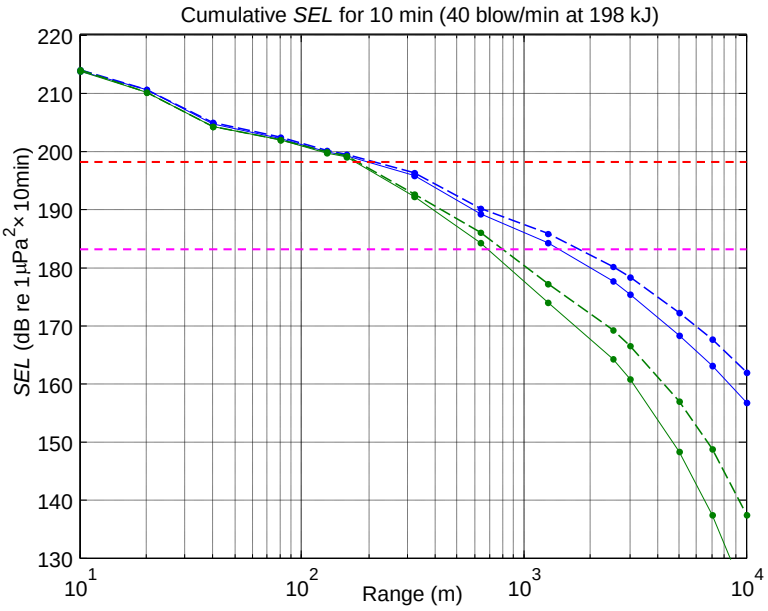


*Figure 4.4: Cumulative sound exposure level for 10 min at a piling rate of 40 blows/min vs range modelled for constant sea depth of 15 m (blue lines) and range dependent bathymetry, shown in Fig.2.11, (green lines) for sound attenuation in the sediment of 0.7 dB/λ (solid) and 0.47 dB/λ (dashed). Red dots show the mean values of measurement data for pile 51-1. Red dashed line shows the level of possible physical injury. Magenta dashed line shows the level of possible TTS onset.*

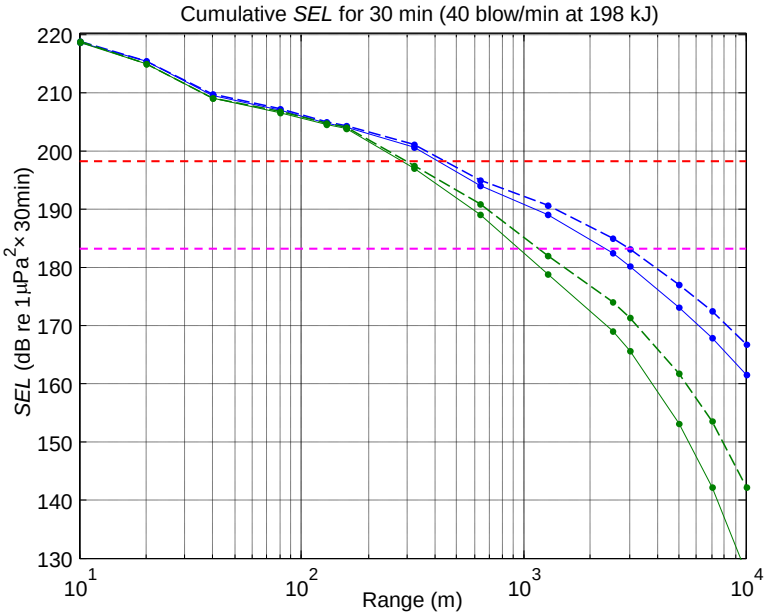


*Figure 4.5: Same as Fig. 4.4, but for 30 min time period.*

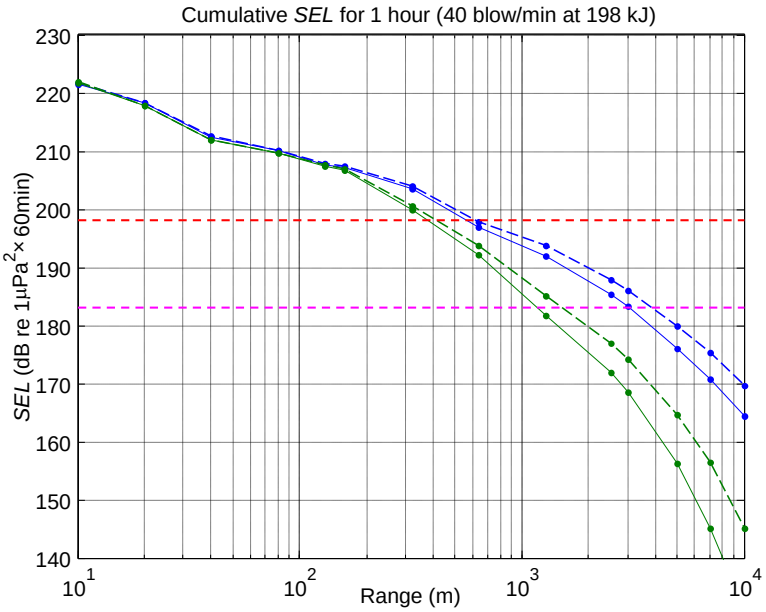


*Figure 4.6: Same as Fig. 4.4, but for 1 hour time period.*

The furthest distance of possible impacts on humpback whales, dolphins and turtles were estimated using the values given in Tables 4.1 and 4.2 and the numerical predictions shown in Figures 4.1 to 4.6. These estimates are summarised in Table 4.3 for humpback whales and dolphins and Table 4.4 for turtles.

*Table 4.3: Furthest distances of various potential impacts of piling noise on humpback whales and dolphins predicted by SVT via modelling and by CMST via modelling verified by measurements.*

| Prediction by: | **Furthest distance of potential physical injury from pile (m)** | | | | | |
|---|---|---|---|---|---|---|
| | Humpback whales | | | Dolphins | | |
| | Exposure duration of: | | | | | |
| | 10 min | 30 min | 1 hour | 10 min | 30 min | 1 hour |
| SVT | 50 | 100 | 250 | 50 | 100 | 250 |
| CMST (vertical piles) | 170 | 300 | 400 | 170 | 300 | 400 |
| CMST (raker piles) | 400 | 600 | 800 | 400 | 600 | 800 |
| | **Furthest distance of TTS - onset from pile to zone (m)** | | | | | |
| SVT | 650 | 1250 | 1800 | 650 | 1250 | 1800 |
| CMST (vertical piles) | 700 | 1000 | 1200 | 700 | 1000 | 1200 |
| CMST (raker piles) | 1300 | 2000 | 2500 | 1300 | 2000 | 2500 |
| | **Furthest distance of possible behavioural disturbance from pile (km)** | | | | | |
| | Humpback whales | | | Dolphins | | |
| SVT | 6 | | | 6 | | |
| CMST (vertical piles) | 7-10 / 6-8.5* | | | 7-10 / 6-8.5* | | |
| CMST (raker piles) | 9-12 / 8-11* | | | 9-12 / 8-11* | | |

* Long-time average $SPL_{RMS}$

*Table 4.4: Furthest distances of various potential impacts of piling noise on humpback whales and dolphins predicted by SVT via modelling and by CMST via modelling verified by measurements.*

| Prediction by: | **Furthest distance of physical injury from pile (m)** | | **Furthest distance of possible behavioural disturbance from pile (m)** | |
|---|---|---|---|---|
| | Adult turtles | Turtle hatchlings | Adult turtles | Turtle hatchlings |
| SVT | 10 | 25 | 700 | n/a |
| CMST (vertical piles) | <10 | 20 | 300 | n/a |
| CMST (raker piles) | <10 | 50 | 600 | n/a |

The predictions of the furthest distances of potential impacts from driven piles on marine animals, including physical injury to the hearing system, TTS onset and behavioural disturbance, made in the SVT reports and in this study are noticeably different for some measures. For example, in this study the furthest distances of potential physical injury are predicted to be several times larger than those predicted by SVT. On the other hand, the furthest distances of TTS onset predicted by SVT are somewhat larger than those estimated in this study. This is not surprising. Firstly, the CMST model of underwater sound emission by impact pile driving is much more physically realistic than the model employed by SVT, where a pile was modelled as a point omnidirectional source placed in the middle of the water column. Secondly, the sound transmission losses modelled by SVT and in this

study seem to be also different, although the transmission loss results are not presented in their report. A strong indication of that difference is a noticeably slower increase of the furthest distance of potential impacts with an increase of sound exposure in the CMST predictions than in the SVT reports. This might take place only if the transmission loss predicted by SVT increased slower with range than the actual transmission loss measured in this study.

### *Multiple piles*

According to the WA Ministerial Conditions (MS 873, Condition 10-17i-c, in Chevron, 2014), underwater noise recordings from concurrent piling of different piles were expected to be included in the library of sound signals from pile driving. During the time period of monitoring from November 2014 to August 2015 only two events of concurrent piling of two different piles were recorded. Figure 4.7 shows a fragment of underwater noise from concurrent driving of piles 46-02 and 56-03 recorded on noise Logger #2 at distances of about 1400 m and 1270 m respectively.

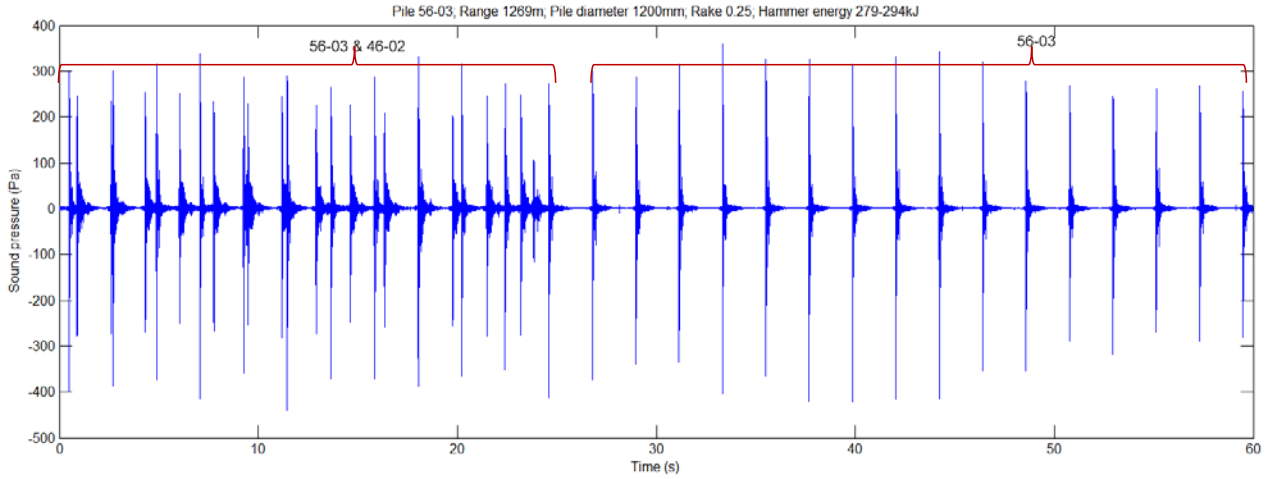


*Figure 4.7: Fragment of underwater noise from concurrent driving of piles 46-02 and 56-03 recorded on Logger #2 at distance of about 1400 m and 1270 m respectively.*

This plot clearly demonstrates that concurrent driving of a number of different piles is unlikely to increase the peak pressure level, because signals from different piles do not constructively interfere with each other. On the other hand, the *SEL* values from multiple piles will be higher, as each pile contributes to the total energy of the sound signal. However, an increase of the *SEL* from multiple piles relative to the *SEL* values from the pile producing the highest level will never exceed $10\log N$, where $N$ is the number of piles concurrently driven, which follows from the energy conservation principle. For $N = 2$, this increase is $\leq 3$ dB.

# 5. Conclusions and future research

## *Conclusions*

1. The physical/numerical model of underwater noise emission from marine impact pile driving developed by the CMST within the scope of this project has been demonstrated to be capable of accurately predicting the major characteristics needed for environmental assessments - sound exposure level and peak and RMS sound pressure levels, which was verified at short and long distances by underwater noise measurements in the Wheatstone piling operation area. The physical model suggested for hammer impact appeared to be adequate for the hammer models used for piling at Wheatstone.
2. It was found from the near-field measurements with 3C seismometers that the seafloor vibrations resulting from interface waves at the water-sediment boundary are insignificant with respect to potential impacts on benthic fauna, compared to vibrations generated by waterborne acoustic waves from pile driving. This is relevant to the environment of the Wheatstone offshore operation area, but may be different in other environments.
3. A library of underwater sounds from marine pile driving in the Wheatstone offshore area has been collected. The library contains sound recordings: (1) at different distances up to nearly 3 km from the piling location, (2) from piles of different size and slant, (3) from two concurrently driven piles, and (4) from piles driven at different hammer energy.
4. A new statistical approach based on extreme value theory has been suggested to predict the peak pressure level and its variations at different distances, so that a threshold can be estimated below which the peak pressure level is expected to fall for a certain probability level.
5. A noticeable difference between sound levels from vertical and slanting piles has been observed. Slanting piles transmit more sound energy in the underwater sound channel in the direction of their bearing and less energy in the opposite direction. In the Wheatstone data, the difference was 10 to 15 dB *SEL*. This should be taken into consideration when assessing potential environmental impacts.
6. The largest distance of various potential impacts of piling noise on the marine fauna of concern have been estimated using the numerical model of sound emission and measurement data. These impacts include: (1) possible injury to animals hearing, (2) TTS onset and (3) behavioural disturbance. Although the estimates made in this study are somewhat different from those made previously by SVT. The difference is not critical in terms of mitigation of possible impacts.
7. One book chapter (Wilkes & Gavrilov, 2016), two journal articles (Wilkes *at al.*, 2016 and Lippert *et al*., 2016) and one referred conference paper (Wilkes *et al*., 2014) have been published based on results of this project. Results of this project have also been used in a PhD study by Marta Galindo Romero at Curtin University.

## *Future research*

1. The physical/numerical model of underwater noise emission from marine impact pile driving can be further improved, if the friction between the pile wall and ground is modelled in an adequate physical way for different types of sediment, including semi or fully consolidated sediments. This may allow more accurate predictions of the sound signal waveform.
2. Physical models of impact force for different types of piling hammer need to be considered.
3. A physical/numerical model of sound emission from slanting piles is needed. It is currently under development at the CMST.

4. Far-field numerical predictions of underwater piling signals over elastic seabeds will require coupling of both pressure and displacement fields in water and ground at a reference distance where modal decomposition is made. An algorithm to implement such coupling needs to be developed.
5. The statistical method for predicting the peak pressure level and its variation needs to be further verified using data from different piles, different environmental conditions and for different driving parameters.

## Acknowledgements

The authors of this and all previous reports on the project gratefully acknowledge the funding of the project provided by Chevron Australia through the Western Australia Energy Research Alliance. In particular, the authors would like to thank Celia Gruenthal and Steven Moore of Chevron for the great organisational, logistic and informational support. The authors also acknowledge all CMST members who have been involved in this project.

# References

Beirlant J., Goegebeur Y., Segers J., Teugels S., and Ferro C.(2004), *Statistics of Extremes: Theory and Applications*. Probabilty and Statistics, ed. J.W.S. Ltd., 2004.

Chevron (2011), Wheatstone Project: "Final Environmental Impact Statement/Response to Submissions on the Environmental Review and Management Programme for the Proposed Wheatstone Project", Vol.2 (Appendix FA) and Vol.3 (Appendix FL).

Chevron (2014), Wheatstone Project: Underwater Noise Monitoring and Review Program.

Deeks A.J, and Randolph M.F. (1993), "Analytical model of hammer impact for pile driving", *Int. J. Numerical and Analytical Methods in Geomechanics*, v. 17, pp. 279-302.

Duncan A., McCauley R., Parnum I., and Salgado Kent C.P. (2010), "Measurement and Modelling of Underwater Noise from Pile Driving", in *20th International Congress on Acoustics, ICA 2010*, Sydney, Australia.

Dyer, I. (1970), "Statistics of sound propagation in the ocean", *J. Acoust. Soc. Am.*, vol.48, pp.337-345.

Galindo Romero M., Lippert T. and Gavrilov A.N. (2015), "Empirical prediction of peak pressure levels in anthropogenic impulsive noise. Part I: Airgun arrays signals", *J. Acoust. Soc. Am EL* 138(6), pp. EL540-EL544.

Gavrilov, A., Duncan, A., and Wu, J.R. (2007), "Geoacoustic inversion from the transmission loss and arrival structure of air-gun signals propagated in deep water", in *Underwater Acoustic Measurements: Technologies & Results, 2nd International Conference and Exhibition*, 2007, Heraklion, Crete.

Gavrilov A.N., Wilkes D. and Gourlay T. (2014), "Modelling underwater noise from marine pile driving: Project progress report32", CMST Report No. 2014-63, Curtin University, Perth WA.

Gavrilov A.N. and Parsons M. J. (2014), "A Matlab tool for the characterisation of recorded underwater sound (CHORUS)", *Acoustics Australia*. 42 (3) pp. 190-196.

Golder Associates (2011), "Wheatstone Phase 3 Downstream Geotechnical Investigation: Final Nearshore Factual Report", Golder Associates Report for Chevron Australia.

Gourlay, T. and Gavrilov, A. (2013), "Modelling underwater noise from marine pile driving: Project progress report 2", CMST Report No. 2013-59, Curtin University, Perth WA.

Jensen, F.B., Kuperman F.A., Porter, M.B. and Schmidt, H. (2011), *Computational Ocean Acoustics*, New York: Springer-Verlag.

Lippert T., Galindo-Romero M., Gavrilov A.N. and von Estorff O. (2015), "Empirical estimation of peak pressure level from sound exposure level. Part II: Offshore impact pile driving noise", *J. Acoust. Soc. Am.* 138(3): p. EL287-EL292.

Lippert S., Nijhof M., Lippert T., Wilkes D., Gavrilov A., Heitmann K., Ruhnau M., von Estorff O., Schafke A., Schafer I., Ehrlich J., MacGillivray A., Park J., Seong W., Ainslie M., de Jong C., Wood M., Wang L., and Theobald P. (2016), "COMPILE - a generic benchmark case for predictions of marine pile driving noise", *IEEE J. Ocean. Eng.* (in production)

PACSYS: FEA / BEM Solutions (2014). Available from: http://www.vibroacoustics.co.uk/

Popper A.N., Carlson T.J., Hawkins A.D., Southall B.L. and Gentry R.L. (2006), "Interim Criteria for Injury of Fish Exposed to Pile Driving Operations" A White Paper.

Reinhall, P.G. and Dahl, P.H. (2011). "Underwater Mach wave radiation from impact pile driving: Theory and observation," *J. Acoust. Soc. Am.*, 130(3), 1209–1216.

Southall B.L., Bowles A.E., Ellison W.T., Finneran J.J., Gentry R.L., Greene Jr. C. R., Kastak D., Ketten D.R., Miller J.H., Nachtigall P.E., Richardson W. J., Thomas J.A., and Tyack P.L. (2007), "Marine Mammal Noise Exposure Criteria: Initial Scientific Recommendations", *Aquatic Mammals*, vol. 33.

Wilkes D.R, Gourlay T.P. and Gavrilov A.N. (2014), "A comparison of numerical methods for the time domain modelling of pile driving noise in the near field", in *Proc. Inter-noise Conf. 2014*, Melbourne, Australia, 16-19 November 2014.

Wilkes D.R. and Gavrilov A.N. (2016), "Numerical Modelling of Sound Radiation from Marine Pile Driving over Elastic Seabeds" in *Fluid-Structure-Sound Interactions and Control*, Zhou, Lucey, Liu and Huang Eds., Springer-Verlag, Berlin Heidelberg 2016.

Wilkes D.R, Gourlay T.P and Gavrilov A.N. (2016), "Numerical modeling of radiated sound for impact pile driving in offshore environments", *IEEE J. Ocean. Eng.* (early access: http://ieeexplore.ieee.org/xpl/login.jsp?tp=&arnumber=7403848&url=http%3A%2F%2Fieeexplore.ieee.org%2Fstamp%2Fstamp.jsp%3Ftp%3D%26arnumber%3D7403848)

## Appendices

The sound library, including sound files, plots of the waveform and a summarising spreadsheet, are provided as separate files.